UNIVERSITAT DE BARCELONA

Immunoreceptor MerTK: A journey from the membrane into the nucleus of human dendritic cells

Kyra J. E. Borgman

Part II:

Membrane receptor MerTK in the nucleus of human DCs

II.1 Introduction

The transmembrane receptor MerTK constitutes together with Tyro3 and Axl the small TAM family within the larger group of receptor tyrosine kinases (RTKs). This surface protein regulates an intriguing mix of seemingly unrelated cellular processes including apoptosis, migration, transcription regulation[1–3] and immunotolerance[4–10]. Physiologically, MerTK is mainly expressed on macrophages and dendritic cells[11], where the receptor plays a role in the phagocytosis of apoptotic cells[5] as well as downregulating the secretion of pro-inflammatory cytokines[12]. Loss of function of the protein leads to inflammation and an increased susceptibility for auto-immune disorders[6,9]. On the other hand, ectopic and overexpression of MerTK has been found in a wide variety of cancers where it activates oncogenic signalling pathways leading to increased cell survival, invasion and therapy resistance [2,3].

MerTK is typically found at the cell plasma membrane and contains an extracellular domain, a single transmembrane domain, and a conserved intracellular kinase domain. The fully mature protein is heavily glycosylated, but partially glycosylated forms of a lower molecular weight are found as well[13]. A soluble form of MerTK also exists, which is the cleaved-off extracellular part of the receptor. This ectodomain can compete for ligand binding with the full receptor and therefore regulate the magnitude of MerTK activation[14]. The membrane-bound receptor is activated by ligand-induced dimerization and subsequent auto-phosphorylation of the kinase domain at several well defined residues[15]. This in turn leads to the phosphorylation of different signalling molecules which can stimulate a wide range of intracellular pathways, depending on cell type and environment. Well studied ligands that can activate MerTK at the cell membrane are ProS[16–18] and Gas6[19,20], while Tubby as well as TULP1[21] and galectin-3[22] have also been identified to induce auto-phosphorylation of MerTK. Cells present in the blood stream are subjected to a high concentration of ProS (~300 nM)[23], while Gas6 is present at ≤0.2 nM in serum and most of this small reservoir is unavailable for MerTK stimulation since it is bound in a complex together with the Axl ectodomain[24]. In the context of dendritic cells (DCs) and tolerance, ProS is the major ligand stimulating MerTK and thereby modulation the magnitude of the immune response[17].

Knock-out studies in mice showed that loss of MerTK increases the susceptibility of the animals to auto-immune disorders[5]. This phenotype is even more pronounced in double and triple knock-out mice missing several members of the TAM family, indicating a tight functional connection between the three family members[6]. The loss of MerTK on both macrophages and DCs is thought to pose the main problem in the knockout mice, resulting

in hampered clearance of apoptotic cells[5,7]. The exposure of the immune system to this disintegrated cellular material in turn leads to inflammation and can induce the formation of auto-antibodies causing auto-immunity. Apoptotic cells typically contain phosphatidyl serine (PS) in their outer leaflet, to which both soluble proteins Gas6 and ProS can bind[19,25]. MerTK-ligand binding then creates a bridge between the antigen presenting cell (APC; both macrophages and DCs fall in this category) and the apoptotic cell, which allows other subsequent mechanisms to properly engulf and clear the dead cell. At the same time, ligand stimulation of MerTK negatively regulates transcription factor NF-κB leading to a decrease in pro-inflammatory cytokine production and therefore downregulation of the immune response[12]. The hampered MerTK signalling in knock-out mice tips the immunological balance between immunity and tolerance towards an over-active immune response that causes harm to its own body. These observations thus clearly implicate MerTK as a very important molecule in establishing immunotolerance, and show that tight regulation of its expression is crucial for a healthy immune response. More recently, a study in human dendritic cells identified MerTK as one of the 50 most upregulated genes in tolerogenic *vs* immunogenic DCs[10]. MerTK upregulation was shown to directly dependent on the tolerogenic treatment with Dexamethasone in a dose-dependent manner[10], suggesting a functional correlation. Tolerogenic DCs (tolDCs), as opposed to immunogenic DCs, are involved in the downregulation of an immune response, and therefore have great clinical potential to counterbalance auto-immune disorders[26]. So far, tolerogenic DCs have been safely used in clinical trials against diabetes type I[27], Rheumatoid Arthritis[28,29] and Crohn's disease[30]. *In vitro* studies identified that tolDCs downregulate the immune response by suppressing both T cell expansion and the production of pro-inflammatory cytokines by T cells[10]. This tolerogenic effect was shown to be associated to MerTK upregulation at the cell surface, since treatment with soluble MerTK-Fc proteins had a similarly suppressive effect on T-cells as tolDCs did[10].

Studies addressing the subcellular localization of MerTK are lacking so far, hampering the further understanding of the molecular mechanisms of action of this intriguing protein. It becomes apparent from the many reports dealing with MerTK, both in the context of cancer as well as auto-immunity and immunoregulation, how important an extensive understanding of the receptor is. The use of TAM receptors as a molecular target in cancer therapy[31–33] as well as the ongoing clinical trials against various auto-immune disorders using tolDCs highly expressing MerTK[27–30] further underline this importance. In this thesis, we used biochemical tools as well as advanced optical imaging techniques, including super-resolution microscopy, to investigate the spatial organization of MerTK on immunogenic and tolerogenic human DCs. Our results show that the receptor is organized in nanoclusters on the plasma membrane of tolerogenic DCs, where it is highly

upregulated. Intriguingly, we discovered a large population of intracellular MerTK that is mainly located in the nucleus. Moreover, nuclear localization of MerTK appears specific for cells of the immune system. Importantly, our work shows that the degree of nuclear localization strictly relates to DC maturation, strongly pointing to a physiological function for the nuclear translocation of a RTK in the context of immunity.

The presence of receptor tyrosine kinases (RTKs) in the nucleus has been reported over the past decade for multiple receptors (reviewed in [34–36]). Amongst these proteins, the EGF receptor (EGFR) is the most well-studied and best known example[37,38]. For many RTKs, including EGFR, nuclear translocation is induced by ligand binding at the membrane level[39–42]. The route for nuclear translocation has been studied as well, and to our knowledge, two major routes have been proposed in the literature for the delivery of surface proteins into the nucleus. The first one describes the role of so-called nuclear envelope-associated endosomes (NAEs) to deliver surface proteins all the way from the membrane to the nucleus[43]. The second route is a reversed version of the pathway that newly synthesized membrane proteins take[37,42]. After endocytosis, the proteins end up in the Golgi and get translocated into the ER via COPI-coated retrograde vesicles[37]. Subsequently, the proteins follow the previously described INTERNET (integral trafficking from the ER to the NE transport) pathway from the ER into the inner nuclear membrane (INM)[42]. Both models however agree on the importance of protein importinβ binding the NLS (nuclear localization sequence) of MerTK in targeting the RTK towards the nucleus. They also both describe the potential role for sec61 β in the final translocation of the receptor across the INM into the nucleoplasm[42,43]. Sec61 β[44] is part of the larger translocon sec61 pore complex that is traditionally involved in inserting newly synthesized transmembrane proteins into the lipid bilayer of the ER. In order to accomplish this, the complex has an opening towards the lumen where the protein can enter, as well as a lateral opening allowing the subsequent incorporation of the protein into the membrane. The EGFR is proposed to follow this process in a reversed manner, being extracted from the membrane through the lateral opening, and released in a soluble form inside the nucleus[42,45].

Translocation of MerTK into the nucleus has never been addressed before. A previous report has mentioned the existence of nuclear MerTK in leukemia cell lines[46], but merely described this observation as a curiosity. The functional impact of nuclear MerTK as well as the mechanism of translocation remains completely elusive. In this thesis, we pave the way for a more fundamental understanding of nuclear translocation of MerTK in human dendritic cells. Using advanced imaging techniques in combination with quantitative analysis, we show that MerTK translocation is triggered by ligand binding, and that it

routes through the ER. We furthermore identify the endocytic receptor LRP-1 as a chaperoning molecule in the partitioning of MerTK over the membrane versus the nucleus, an entirely novel role for this receptor. The identification of LRP-1 as a nuclear chaperone may have a great impact on the study of other RTKs in the nucleus, as well as providing a potentially new molecular target for the clinical interference in this oncogenic process.

Since the translocation of RTKs into the nucleus has been so far mostly associated with malignant overexpression of the receptors, the scientific community has been rather reluctant to assign any importance to this mechanism. However, it is becoming increasingly clear that nuclear RTKs can indeed have a biological function within the nucleus. Both the EGFR and the RON receptor have been shown to function as transcription factors and several of their target genes have been identified, which are in most cases associated to cell proliferation[39,47,48]. The EGFR has furthermore been implicated in the phosphorylation of PCNA[49,50], which is an important protein in the regulation of replication and DNA repair. Increased proliferation further potentiates the oncogenic phenotype of tumours overexpressing the EGFR, and augmented DNA repair poses an advantage in resistance to chemotherapy. Given the very fundamental cellular processes in which nuclear RTKs are involved, and the extensive consequences upon misregulation, further studies in this field are of vital importance. In this thesis, we took the critical first steps in identifying the function of nuclear MerTK. Using super-resolution imaging, we characterized the spatial relationship between MerTK and the chromatin in human DCs. We show that MerTK preferentially localizes to heterochromatin, avoiding the dense euchromatin at the nuclear periphery. Additionally, we also show that MerTK accumulation to the nucleus is much stronger when the DCs hold their chromatin in a more open conformation during early stages of differentiation, compared to MerTK accumulation to the nucleus of fully differentiated DCs in which the chromatin in denser. This localization profile suggests that MerTK is involved in the regulation of transcriptionally active genomic regions. Altogether, our results suggest a physiological role for nuclear MerTK in non-proliferating immune cells related to DC differentiation, possibly as a transcription factor.

II.2 Objectives

The transmembrane receptor MerTK has been described as an important receptor in immunoregulation. By facilitating phagocytosis of apoptotic cells without the generation of an immune response[5], this receptor in crucial in keeping the immune system from harmful over reactivity to self-material. In addition, MerTK suppresses T cell proliferation[10] and the secretion of pro-inflammatory cytokines[10,12]. Loss of MerTK in knock-out mice leads to inflammation and auto-immunity[5,9]. On the other hand, MerTK overexpression has been reported in many different types of tumours, where it activates oncogenic signalling pathways involved in cell survival, invasion and therapy resistance [2,3]. Because of its involvement in immunotolerance as well as in cancer, MerTK represents a very clinically attractive molecule. Currently, MerTK[51] and other TAM receptors[31–33] are used as a molecular target in various cancer therapies. In addition, several clinical trials using tolerogenic dendritic cells that highly express MerTK to fight auto-immune disorder have been recently published [27–30].

It is thus of utmost importance to fully understand the molecular mechanism of action of MerTK. Although the function of this receptor has been well characterized in various biological contexts, its subcellular organization remains completely elusive. Many studies over the past decades have made it increasingly clear that there is a tight interconnection between spatiotemporal organization of immunoreceptors at the nanoscale and their function[52–55]. In this thesis, we therefore aimed to unravel the spatial distribution of MerTK in human dendritic cells (DCs) to further the understanding of its molecular functioning.

In consequence, the objectives of this doctoral thesis were the following:

1) Mapping the spatial organization of MerTK on the membrane of tolerogenic DCs.
2) Characterizing the intracellular pool of MerTK found in tolerogenic as well as immunogenic DCs, by studying its exact subcellular localization.
3) Identifying the role of ligand binding and thus receptor activation in the subcellular distribution of MerTK.
4) Determining the interaction and spatial relation between intracellular MerTK and other proteins of interest in order to uncover the function of the membrane receptor in this non-classical location.

II.3 Methodology

Cell Culture

Dendritic cells were derived, as reported previously[56], from peripheral blood samples. Buffy coats from healthy donors were obtained from *Banc de Sang I Teixits* upon written informed consent. In brief, peripheral blood mononuclear cells (PBMCs) were allowed to adhere to a plastic surface for 2 h at 37°C. Unbound PBMCs were washed away, and the remaining adherent monocytes were cultured for 48h in the presence of IL-4 (300 U/ml) and GM-CSF (450 U/ml) (both from Miltenyi Biotec, Madrid, Spain) in X-VIVO 15 (BioWhittaker, Lonza Belgium) medium supplemented with 2% AB human serum (Sigma-Aldrich, Spain). At that moment, they are day 0 DCs, and were used for several experiments. To generate iDexs, the cells were further cultured for 4 days in the same conditions plus Dexamethasone ($10^{=6}$ M; MERCK). IDCs were equally generated in 4 days, but without the extra addition of Dex.

THP-1 cells were cultured in RPMI 1640 medium supplemented with antibiotic-antimycotic (both Gibco) and 10% FBS (ThermoFisher). To induce a DC-like phenotype, they were cultured for 6 days in the presence of IL-4 and GM-CSF, with a medium exchange after 3 days.

Antibodies and specific reagents

The following primary antibodies were used throughout this study at a concentration of 5 ug/ml, expect for the STORM experiments where they were used at a concentration of 20 ug/ml: α-MerTK (mouse extracellular monoclonal, 125618, R&D Systems), α-MerTK (goat extracellular polyclonal, AF891, R&D Systems), α-MerTK (rabbit extracellular monoclonal, Y323, Abcam), α-MerTK (rabbit intracellular polyclonal phosphospecific, PMKT-14GAP, FabGennix), α-ProS-AF647 (bs-9512R-A647, Bioss), α-LAMP1 (H5G11, Santa Cruz Biotechnology), α-calreticulin (ADI-SPA-601, Enzo), α-EEA1 (14/EEA1, BD Biosciences), α-LRP-1 (LRP1-11, Sigma-Aldrich), α-PanHis (H11-4, Merck Millipore), α-H2B (5HH2-2A8, Merck Millipore), α-HDAC1 (10E2, Cell Signalling), α-tubulin (YL1/2, Abcam).

For confocal and STED imaging, the following secondary antibodies were used, all at a concentration of 10ug/ml: Goat-α-mouse-AF488 (A11001, ThermofFisher), Goat-α-mouse-Atto647N (50185, Sigma-Aldrich), Goat-α-rabbit-AF488 (A11008, ThermoFisher), Goat-α-rabbit-AF647 (A21244, ThermoFisher).

For western blot imaging, the following secondary antibodies were used (all from ThermoFisher): Donkey-α-rabbit-AF680 for MerTK, Donkey-α-mouse-AF680 for HDAC1 Donkey-α-rat-DyLight800 for tubulin.

For STORM imaging, the secondary antibodies (donkey-α-mouse and donkey-α-rabbit from ImmunoResearch, used at a concentration of 20 ug/ml) were labelled in-house with different combinations of pairs of activator/ reporter dyes. The dyes were purchased as NHS ester derivatives: Alexa Fluor 405 Carboxylic Acid Succinimidyl Ester (Invitrogen), Cy3 mono-Reactive Dye Pack (GE HealthCare), and Alexa Fluor 647 Carboxylic Acid succinimidyl Ester (Invitrogen). Antibody labelling reactions were performed by incubating a mixture of secondary antibody, NaHCO3, and the appropriate pair of activator/reporter dyes diluted in DMSO for 40 min at RT. Purification of labelled antibodies was performed using NAP5 Columns (GE HealthCare). The dye to antibody ratio was quantified using Nanodrop and only antibodies with a composition of 3-4 Alexa Fluor 405 and 0.9-1.2 Alexa Fluor 647 per antibody were used for imaging.

Recombinant human PROS1 (R&D systems, 50 nM final concentration) and recombinant human RAP (Merck Millipore, 200 nM final concentration) were used to stimulate nuclear translocation of MerTK.

Flow Cytometry

For flow cytometry analysis, DCs were labelled with primary antibody α-MerTK (R&D systems), followed by secondary staining with PE-labelled goat-anti-mouse (from BD Biosciences), both for 30 min at 4°C and a concentration of 5 µg/ml. Appropriate isotype control IgG1 (from BD Biosciences), was included. Flow cytometry was performed using FACSCanto II.

MerTK transfection

HeLa cells were transfected using TransIT-HeLaMONSTER and HEK293 cells using TransIT-293 (both from Mirus). The pCMV3-MERTK plasmid was purchased from Sino Biologicals. Cells after transfection were cultured both with and without ProS or HS in the medium, to potentiate nuclear translocation of MerTK. Cells were typically imaged 24h after transfection, although both earlier and later time points were explored as well.

Cell fractionation and western blot detection

Dendritic cells at day 0 and DC-like THP-1 cells were collected and fractionated into the cytoplasmic fraction, the soluble nuclear fraction and the chromatin bound fraction following Wang et al.[57]. In brief, cells were crushed using a Dounce tissue grinder set (Sigma-Aldrich) of 2ml, which homogenizes the cells without rupturing the nuclear membrane. Effectivity of this step was checked under the microscope with a Trypan Blue staining. Cytoplasmic material was then separated from the intact nuclei by centrifugation. The nuclei were subsequently lysed, and the chromatin was separated from the soluble fraction by centrifugation. The chromatin pellet was then sonicated in order to release associated proteins and allow their detection. All 3 fractions were then loaded and ran, transferred, and stained following standard western blotting procedure. Besides for MerTK, we also stained for tubulin and HDAC1 to verify the effectiveness of the cell fractionation.

Sample preparation for fluorescence imaging

Fresh cells were diluted up to a concentration of 1×10^6 per ml in plain medium, and attached to the bottom of the cover glasses (Lab-Tek) by incubation for 30 min. Then, samples were fixed using 4% paraformaldehyde (PFA) for 15 min at RT. Then, cells were blocked and permeabilized for 1h at RT with 3% BSA and 0,5% TritonX-100 in PBS, followed by primary and secondary labelling both for 30 min at RT. Finally, all samples were fixed again with 2% PFA and stored at 4 °C. For membrane stainings, TritonX-100 was left out from the blocking mixture.

Confocal imaging

Imaging was performed using a confocal microscope (TCS SP5, Leica Microsystems). Images were taken with a 1.4 NA oil immersion objective (HCX PL APO CS 63.0x, Leica), a 512×512 pixels format and a scanning speed of 400 Hz. AF488 was excited with the 488 nm line, at 25% of the argon laser power and detected between 500 nm and 570 nm. Atto647N or AF647 was excited with the 633 nm line at 30% of the HeNe laser power and detected between 645 nm and 715 nm. To be able to use the fluorescence intensity measurements in a quantitative way, imaging conditions were always kept constant across measurements, and a calibration sample was used to account for day to day fluctuations in the system.

STED imaging

Imaging was performed using a commercial STED microscope (TCS SP5, Leica Microsystems). Images were taken with a 1.4 NA oil immersion objective (HCX PL APO CS 63.0x, Leica), a 1024×1024 pixels format and a scanning speed of 1400 Hz. The effective imaging beam was constituted of the 488 nm line, at 25% of the argon laser power, and 100% of the depletion donut-shaped laser at 592 nm. Fluorescence was collected between 500 nm and 570 nm. The resolution was around 100 nm, as determined by fitting the fluorescence profile of single primary antibodies on the glass to a Gaussian curve, and taking it's full-width-half-maximum (FWHM). The size of actual MerTK clusters on the cell was determined in a similar way. The number of molecules per cluster was determined by manually selecting both fluorescent spots on the cells and on the glass, establish their peak fluorescence intensity, and dividing the fluorescence of the actual clusters by the fluorescence coming from the single primary antibodies on the glass. All of this was done using a custom written code in Matlab.

STORM imaging

STORM (Stochastic Optical Reconstruction Microscopy) imaging takes advantage of the on-off photoswitching properties of individual fluorophores to localize them with nanometric precision. The method is based on the repeated imaging of sparse stochastic subsets of fluorophores in the sample. The positions of active fluorophores are determined by finding the centres of their point spread function, and then used to construct a super-resolution image of the labelled structure with an effective resolution around 20nm.[58]

In this study, a commercial microscope system from Nikon Instruments (NSTORM) was used. Samples were prepared as described above, and imaged in the following buffer to facilitate blinking: Cysteamine MEA (Sigma-Aldrich), Glox Solution (0.5 mg/ml glucose oxidase, 40 mg/ml catalase; both Sigma Aldrich), 10% Glucose in PBS[59]. Images were acquired with a frame rate of 83 frames per second. In single colour experiments, H2B was stained with the AF405-AF647 activator/reporter dye pair. By exciting AF405 with the corresponding laser line at 405 nm, this dye becomes activated and transfers its photons to the reporter dye. The reporter dye in turn will emit these photons only upon excitation with a 647 nm laser, and subsequently goes back into the dark state. We therefore used an imaging cycle in which one frame belonging to the activating light pulse (405 nm) was alternated with 3 frames belonging to the imaging light pulse (647 nm). Dual colour imaging was performed with two sets of secondary antibodies labelled with the same reporter dye (Alexa Fluor 647) but two different activator dyes (Alexa Fluor 405 for MerTK and Cy3 for panHis)[59]. In addition to the first imaging cycle of 4 frames, a

second cycle of again 4 frames, but with an activation laser pulse at 561 nm, was used to image Alexa Fluor 647 linked to activator Cy3.

In order to exhaustively image all fluorophores in a reproducible manner allowing for quantitative comparison across cells and conditions, we used the following scheme to increase the activator laser power, according to Ricci et al.[60].

Activating laser power	frames
8 mW	Until 20.000
9 mW	20.000 - 37.000
10 mW	37.000 - 50.000
11 mW	50.000 - 57.000
13 mW	57.000 - 63.000
15 mW	63.000 - 70.000
18 mW	70.000 - 75.000
22 mW	75.000 - 80.000
29 mW	80.000 - 85.000
38 mW	85.000 - 90.000
48 mW	90.000 - 95.000
60 mW	95.000 - 100.000

STORM image processing

Grouping of the x-y localization into clusters was done according to Ricci et al.[60]. First, a density map was generated, in which each pixel has a value equal to the number of localizations falling within the pixel area (pixel size = 10 nm). A constant threshold was then used to convert the density maps into binary images, such that pixels have a value of 1 where the density is larger than the threshold and a value of 0 elsewhere. Localizations falling on zero-valued pixels were discarded from further analysis. For our threshold setting, the number of discarded localizations typically corresponded to < 5% of the total number of localization within a nuclear region. Connected components of the binary image, composed by adjacent non-zero pixels (4-connected neighbours), were sequentially singled out and analysed. Localization coordinates within each connected component were grouped by means of a distance-based clustering algorithm. Initialization values for the number of clusters and the relative centroid coordinates were obtained from local maxima of the density map within the connected region, calculated by means of a peak finding routine. Localizations were associated to clusters based on their proximity to cluster centroids. New cluster centroid coordinates were iteratively calculated as the average of localization coordinates belonging to the same cluster. The procedure was iterated until convergence of the sum of the squared distances between localizations and

the associated cluster and provided cluster centroid positions and number of localizations per cluster. All was done by means of a custom written code in Matlab.

Image analysis

All image analysis was performed using ImageJ unless otherwise stated. Nuclear MFI was quantified by manually selecting the nuclear area based on wide field images of the cells. Colocalization was determined using the plugin Coloc2, and quantified either by using the Pearson correlation coefficient for raw images, or the Mander's overlap coefficient for binary images. Image segmentation was performed according to Rizk et al[62], using their plugin.

Statistical Analysis

All analyses were performed using GraphPad Prism 6. Results are shown as the mean ± SD. To determine statistical differences between the mean of two data sets, the (un)paired two-tailed Student T-test was used. To determine statistical differences between the mean of 3 or more data sets, the One-way ANOVA was used, followed by the Tukey's multiple comparison test. Significance is represented using: *ns (*$P>0.05$); * ($P<0.05$); ** ($P<0.001$) and *** ($P<0.0001$).

II.4 Results

MerTK is organized in nanoclusters on the plasma membrane of tolerogenic DCs

Recent studies by Cabezon et al[10] showed that MerTK is highly upregulated on immature tolerogenic DCs at the mRNA level as well as in surface expression of the protein. This upregulation is directly controlled by the tolerogenic treatment for 4 days with Dexamethason (Dex) in a dose-dependent manner. The MERTK gene is one of the 50 most upregulated genes in tolerogenic versus immunogenic DCs, making MerTK an attractive protein to study in order to understand the tolerogenic phenotype of DCs. We first confirmed using flow cytometry that immature dendritic cells treated with Dex, referred to as iDex, highly express MerTK on their plasma membrane as opposed to immunogenic immature DCs (iDCs). We indeed obtain a three-fold increase in surface expression of the receptor upon tolerogenic treatment (Fig. II.1 A). To map the distribution of the receptor at the single cell level, we performed stimulated emission depletion (STED) nanoscopy imaging. This imaging technique provides a lateral spatial resolution better than 100 nm, i.e., a three-fold resolution increase as compared to diffraction limited confocal microscopy (see Part I for an overview of the technique). A representative STED image of labelled MerTK expressed on the surface of an iDex cell is shown in Fig. II.1 B. The increased resolution brought about by STED allowed us to resolved well-defined fluorescence spots of MerTK homogeneously distributed over the plasma membrane (Fig. II.1 B). Multiple images from different iDex cells were analysed by measuring the brightness of individual MerTK spots on the cell membrane. For comparison, the brightness of individual fluorescent spots of non-specifically adsorbed anti-MerTK Abs scarcely found on the substrate next to the cell surface were also measured. Since the fluorescence spots on the glass coverslip most probably represent individual Abs[52,54], we used their average intensity to quantify the number of MerTK molecules contained in each spot. We estimate that the spots on the membrane are small MerTK nanoclusters consisting of on average 3 and up to 10 receptors each (Fig. II.1 C). In addition, the physical size of the spots was determined by measuring the full-width-at-half-maximum (FWHM) of a Gaussian fit to the intensity profile of each single spot. The effective STED resolution under our imaging conditions was determined by measuring individual spots on glass and resulted around 100 nm (Fig. II.1 D). MerTK nanoclusters are around 120nm in size (Fig. II.1 D), clearly between the resolution limits of traditional confocal imaging and STED nanoscopy. The kind of organization we report here for MerTK fits nicely with the general consensus that nanoclusters are the functional unit for many immunoreceptors on the plasma membrane [52–55].

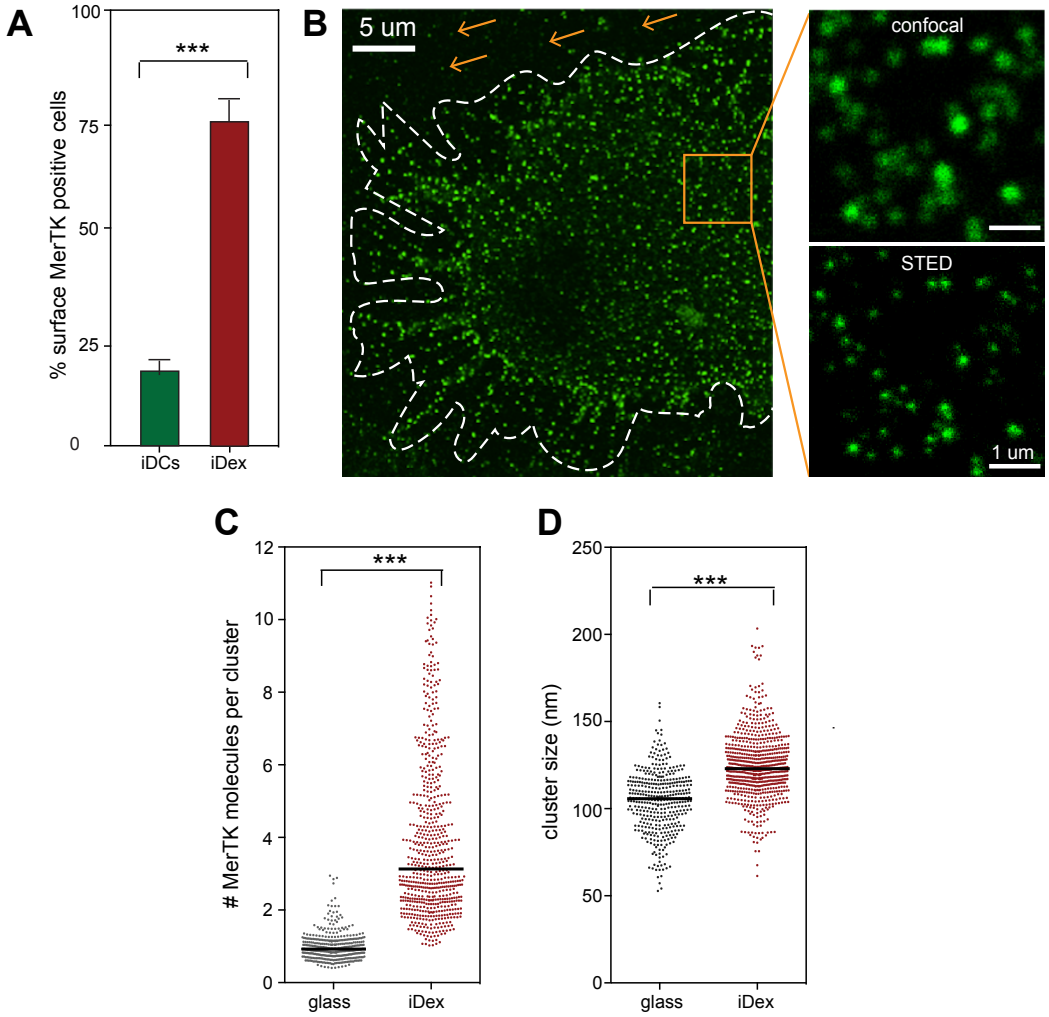

Figure II.1: Distribution of MerTK on the membrane of iDexs. (**A**) Flow cytometry analysis of surface MerTK expression on iDC and iDex cells (n=8). (**B**) Representative STED image of MerTK labelled on an iDex cell. The dotted line delineates the cell, while the orange square indicates the location of the zoom-in images, that are represented in confocal and STED mode to show the increase in resolution using STED. The orange arrows point to individual 'labelling unit' on the glass that are used for the quantification in C. (**C**) Number of MerTK molecules per cluster in iDexs, calculated by dividing the fluorescence intensity of each MerTK spot by the average intensity of the spots on the glass (single labelling units of 1 primary and several secondary antibodies). Data from 3 different donors (around 8 cells each) was pooled. (**D**) Physical size of MerTK clusters in nm, calculated by taking the FWHM of the fitting of the fluorescence intensity profile of each spot. The size of the spots on the glass represent the resolution limit of our STED system, around 100 nm. Data from 3 different donors (around 8 cells each) was pooled.

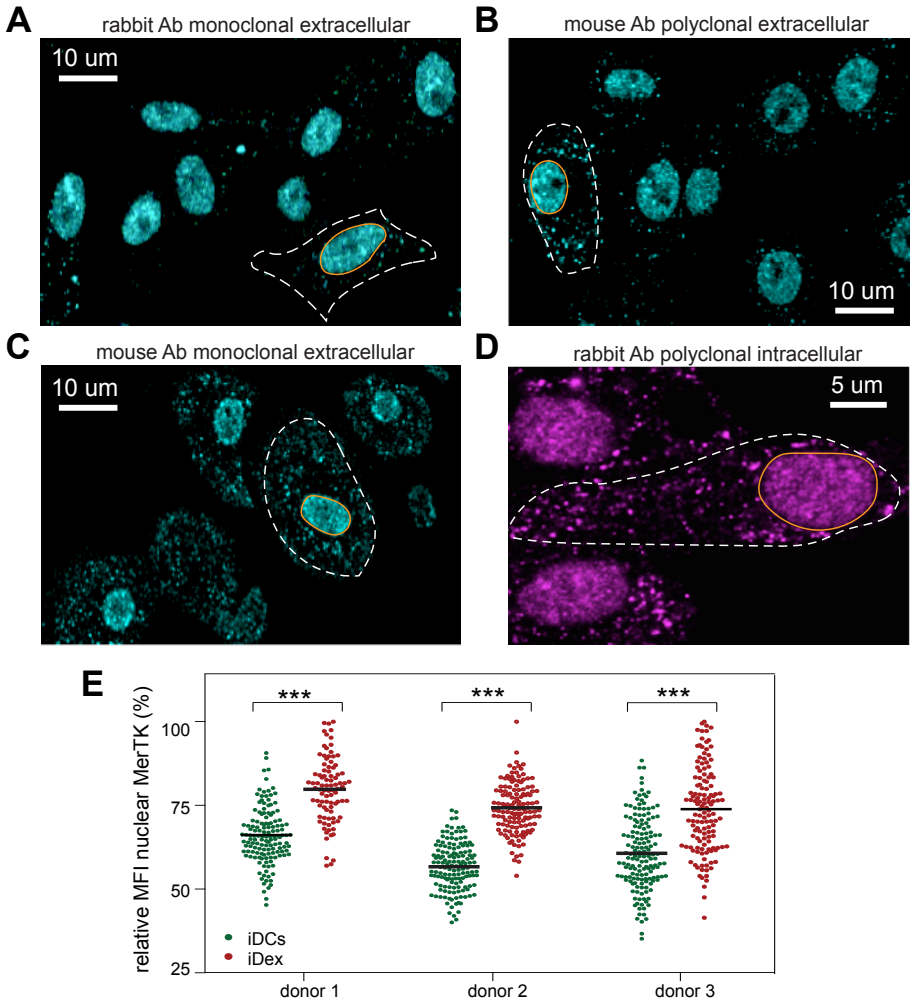

Figure II.2: Intracellular distribution of MerTK in DCs. (**A-D**) Representative confocal images of the intracellular distribution of MerTK in permeabilized iDex DCs, using various anti-MerTK antibodies. Clear nuclear localization of MerTK becomes apparent in all cases. The dotted line represents the cell boundary, while the orange line represents the nuclear envelope. (**A**) rabbit monoclonal antibody against an extracellular epitope of MerTK (**B**) mouse polyclonal antibody against an extracellular epitope of MerTK (**C**) mouse monoclonal antibody against an extracellular epitope of MerTK (**D**) rabbit polyclonal antibody against the intracellular domain of MerTK. (**E**) Quantification of the mean fluorescence intensity (MFI) of MerTK in the nucleus of iDCs and iDexs. MFI (mean fluorescence intensity) was calculated using imageJ by manually selecting the nuclear area based on bright field images. Data was normalized, per donor condition, to the highest value obtained in iDex DCs for that particular donor. This was done to facilitate comparison between donors, since not all experiments were performed using the same secondary fluorophore-conjugated antibodies. Each dot represents an individual nucleus (around 80-100 cells per donor per condition).

The intracellular pool of MerTK almost entirely resides in the nucleus

A significant intracellular pool of MerTK of around 40% of the total protein level was previously picked up by flow cytometry in different types of DCs[10]; an abnormally high amount for a membrane receptor. We therefore characterized the subcellular distribution of intracellular MerTK by confocal microscopy. Unexpectedly, we found that this pool almost entirely resides inside the nucleus (Fig. II.2 A). Probing MerTK with two more anti-MerTK antibodies against different extracellular epitopes and produced by different manufacturers gave the exact same phenotype, validating the specificity of the antibodies (Fig. II.2 B, C). A fourth anti-MerTK antibody staining the intracellular domain of the receptor again gives a similar nuclear profile (Fig. II.1 D). The presence of both the intracellular as well as the extracellular domain of MerTK in the nucleus strongly suggests that the entire intact protein is translocated, including its transmembrane domain. Similar nuclear localization of MerTK was also observed on iDCs, although iDexs exhibited more pronounced accumulation in the nucleus as compared to iDCs (Fig. II.2 E). These results thus indicate that MerTK nuclear localization is a property of immature DCs, regardless of tolerogenic treatment. Together with the results shown in Fig. II.1 A, these data further suggest that MerTK upregulation upon Dex treatment mainly leads to membrane-bound MerTK without significantly increasing the pool of nuclear MerTK.

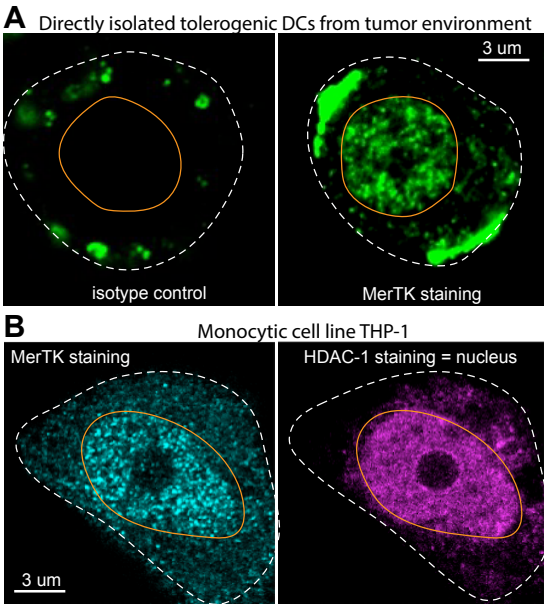

Figure II.3: Nuclear MerTK in different monocytic immune cells. (**A**) Representative confocal image of a permeabilized tolerogenic DC directly isolated from the tumour environment of a cancer patient. The cell is stained for MerTK, and nuclear localization becomes apparent, while this is not the case for the isotype control. (**B**) Representative confocal image of a permeabilized THP-1 cell (monocytic cell line) stained for MerTK. The nuclear area is identified using HDAC-1 staining, since the cell nucleus is not easily identifiable from bright field images due to the rounded shape of monocytes. Again, the nuclear localization of MerTK becomes apparent. The dotted lines highlight the cell boundary; the orange lines represent the nuclear envelope.

To further validate our results obtained on *in vitro* differentiation of tolerogenic DCs, we isolated immune cells with a tolerogenic phenotype directly from the tumour environment and recovered similar nuclear MerTK distribution (Fig. II.3 A). Nuclear localization was also observed in the monocytic cell line THP-1 (Fig. II.3 B). All together, these results thus show clear nuclear localization of MerTK in different types of immune cells: cells from the THP-1 monocytic cell line, *in vitro* monocytic derived DCs and directly isolated tolerogenic DCs.

Nuclear MerTK appears a specific treat for immune cells

The presence of several other RTKs in the nucleus has been widely reported over the last decade, but almost exclusively as a malignant side effect of its overexpression in tumour cells[34,38,63]. We therefore sought to investigate whether the same would hold for MerTK, by aberrantly or overexpressing the receptor in different tumour cell lines. HeLa cells transfected with MerTK show a cell membrane expression profile similar to that on iDexs with the presence of small nanoclusters (Fig. II.4 A). This ectopic expression however did not lead to nuclear translocation of MerTK (Fig. II.4 B). Likewise, HEK293 cells that endogenously express MerTK do not show nuclear expression of MerTK (Fig. II.4 C), and overexpression of MerTK is this cell line does not induce nuclear translocation of the receptor either (Fig. II.4 D). This treat seems exclusively reserved for immune cells

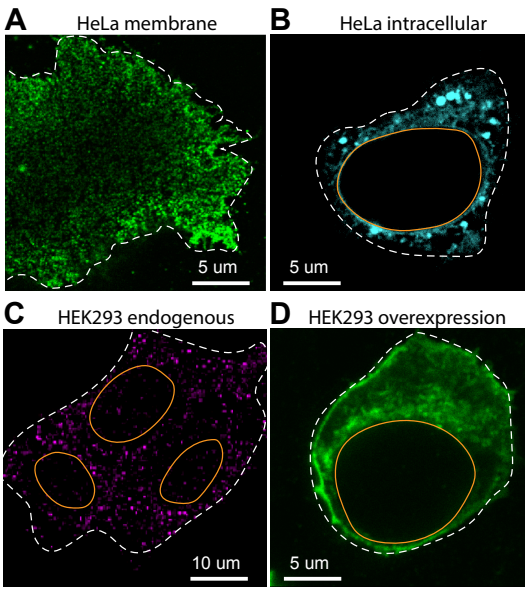

Figure II.4: Localization of endogenous and ectopic MerTK in other cell types.

(**A**) Representative confocal image of a MerTK transfected HeLa cell stained for MerTK on the membrane. Clustering of the receptor like on the membrane of iDexs becomes apparent, indicating a successful transfection and correct incorporation of the transmembrane domain. (**B**) Representative image of a MerTK transfected HeLa cell, permeabilized and stained for MerTK intracellularly. No nuclear localization of MerTK is observed. (**C**) Representative image of permeabilized HEK293 cells stained for MerTK. Cells endogenously express MerTK, but it is not found in the nucleus. (**D**) Representative image of a HEK293 cell after transfection with MerTK to induce overexpression of the protein. Even though a clear increase in the intracellular MerTK level is observed, nuclear localization is not observed.

(THP-1, several types of DCs, Jurkat T cells[46]). Our data thus show that the presence of nuclear MerTK is not a result of aberrant overexpression of the receptor as is the case for many other RTKs, but uniquely indicates a physiological role for nuclear MerTK in immune cells.

The amount of nuclear MerTK strictly relates to DC differentiation

Membrane expression of MerTK was previously shown to be clearly dependent on tolerogenic treatment with Dexamethasone[10]. Surface MerTK steeply increases in the first two days after addition of the glucocorticoid, while iDCs that differentiate equally during those days but in the absence of Dex do not show a significant increase in MerTK expression[10]. We therefore sought to investigate whether the same dependence holds for the nuclear level of MerTK. For this, we measured the amount of nuclear MerTK during each of the seven days of differentiation from monocytes into iDCs or into iDexs by confocal imaging (Fig. II.5 A). Interestingly, we observe that tolerogenic treatment is not the main factor influencing the amount of nuclear MerTK, as expression levels are comparable in the presence or absence of Dex treatment (Fig. II.5 A) with only a modest but significant difference at day 4 (last time point in Fig. II.5 A highlighted by a red arrow and Fig. II.2 E). Instead, a very clear dependence between the amount of nuclear MerTK and the stage of differentiation becomes apparent, which is maximum at day 0, the moment when morphological changes can be observed that indicate the transition of monocytes into early DCs. Focusing in more detail on the exact subcellular distribution of intracellular MerTK during the transition period, we observe that it is highly expressed throughout the entire cytoplasm around day -1 (Fig II.5 B second panel). At the next stage, specific accumulation into the nucleus seems to be initiated around day 0 (Fig II.5 B third panel), which continues and leads to a well-defined phenotype where almost all the intracellular MerTK resides in the nucleus (Fig. II.5 B last panel).

To further demonstrate that this increase in nuclear MerTK expression is indeed specific for the differentiation of the cells rather than days of *in vitro* culturing, we investigated the effect of the differentiation cocktail (cytokines IL-4 and GM-CSF that together facilitate the differentiation of monocytes into DCs[56]) on the amount of nuclear MerTK. First, we used different doses of IL-4 to transition monocytes into day 0 DCs. As expected, the higher the dose of this differentiating cytokine (within the physiological relevant range of DC differentiation), the more MerTK accumulates into the nucleus (Fig. II.5 C), indicating a causative relation between differentiation and nuclear MerTK.

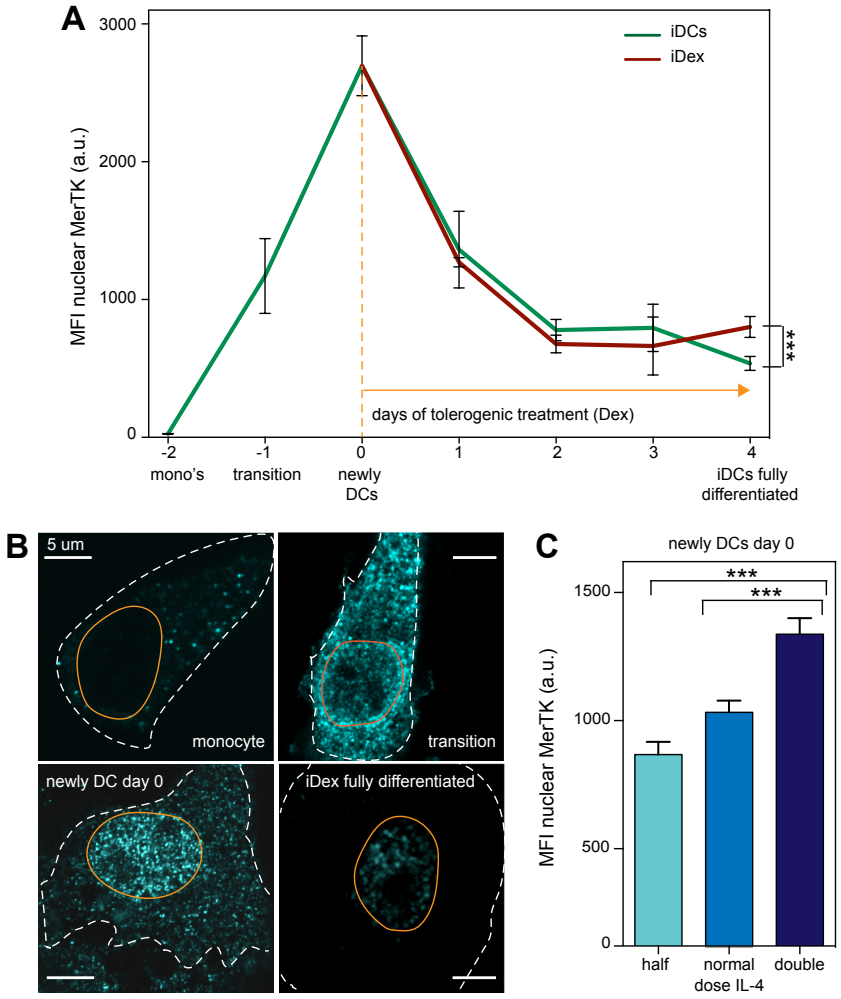

Figure II.5: Amount of nuclear MerTK during DC differentiation. (**A**) Quantification of nuclear MFI of MerTK at different time points during monocyte differentiation into DCs. Day -2 correspond to monocytes harvested for imaging several hours after removal of all other leukocytes and day -1, correspond to transition cells from monocytes into DCs. Day 0 corresponds to the moment in which monocytes become newly DCs. At day 0, Dex was added to the cells destined to become iDexs, while iDCs were allowed to further differentiate without Dex. IL-4 and GM-CSF were always present in the medium to promote differentiation. 25-50 cells from 3 different donors per condition were measured. (**B**) Representative confocal images of intracellular MerTK distribution in differentiating monocytes at different time points. The dotted line represents the cell boundary, while the orange line represents the nuclear envelope. (**C**) Nuclear MFI of MerTK as a function of the dose of IL-4 during the first 2 days of differentiation (day -2 to day 0). Monocytes were cultured in the presence of different doses of IL-4 during 2 days to access the direct effect of IL-4 on the nuclear accumulation of MerTK. Per condition, around 80 cells from 2 different donors were measured.

Second, we administered the full differentiation cocktail to the THP-1 monocytic cells, that had previously been cultured already for several cell cycles. A clear change of cell morphology was observed (Fig. II.6 A-C), which agrees with the notion that the monocytes acquired a DC-like phenotype, as reported previously[64,65]. In addition, a very strong increase in nuclear expression of MerTK was observed as a result of the differentiation (Fig. II.6 D). Altogether these findings demonstrate that the degree of nuclear MerTK expression is strictly dependent on DC differentiation, and it is at its maximum at the transition period from monocytes into early DCs. This suggests that unlike other RTKs in the nucleus, MerTK has a physiological nuclear function, which is related to the maturation of DCs.

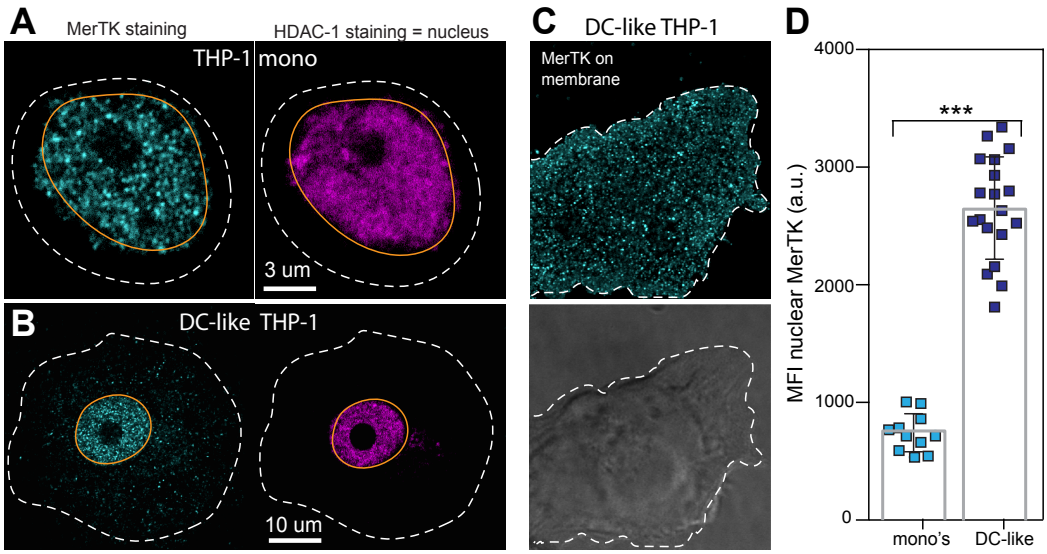

Figure II.6: Nuclear MerTK increases upon THP-1 differentiation. (**A**) Representative confocal image of a permeabilized THP-1 cell (monocytic cell line) stained for MerTK. The nuclear area is identified using a HDAC-1 staining, to facilitate the identification of the nucleus on monocytes. Clear nuclear localization of MerTK is observed. The dotted line represents the cell boundary; the orange line represents the nuclear envelope. (**B**) Representative confocal image of a permeabilized THP-1 cell that has been differentiated into a DC-like phenotype, stained for MerTK. The nuclear area is identified using a HDAC-1 staining. Again, nuclear localization of MerTK is observed. (**C**) Representative confocal image (upper row) of a DC-like THP-1 stained for MerTK on the membrane. Clustering of the receptor similar to that observed on the membrane of iDexs is apparent, as well as flattening of spreading of the cell, characteristic of DC phenotype (bright-field image, bottom row). (**D**) Quantification of nuclear MFI of MerTK in THP-1 cells before and after differentiation towards a DC-like phenotype. N=20.

Binding of ligand ProS induces nuclear translocation of MerTK

Trafficking from the membrane into the nucleus has previously been reported for several tens of RTKs[34,35], amongst which the EGFR is the most well-studied[37,38]. For many RTKs, nuclear translocation is triggered by ligand binding at the membrane level[39–42]. This prompted us to explore the role of ligand ProS[17,66,67] in the nuclear translocation of MerTK. We therefore performed dual colour confocal imaging of both MerTK and ligand ProS to study their interaction. Overall, we show a strong colocalization between both proteins intracellularly (Fig. II.7 A).

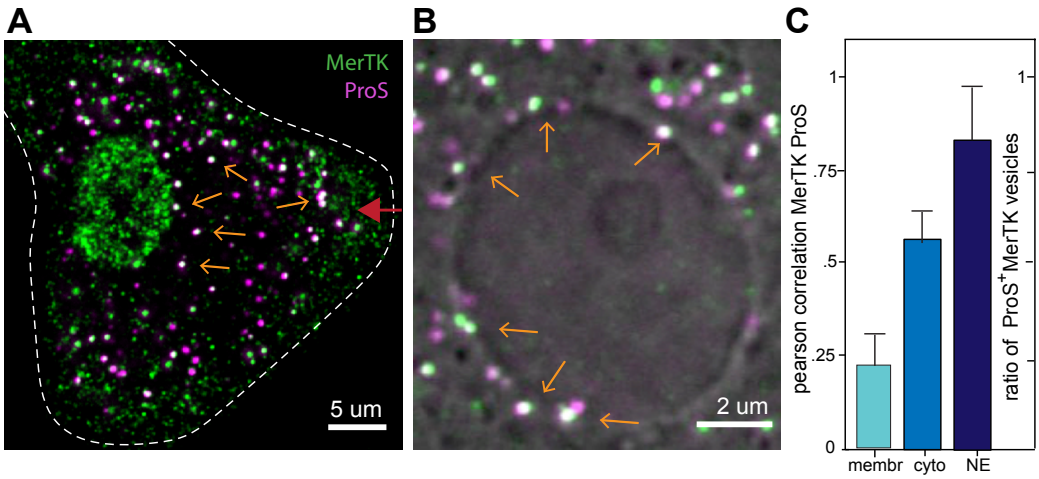

Figure II.7: Ligand ProS and MerTK colocalize intracellularly, especially at the NE (A) Representative dual colour confocal image of MerTK and its ligand ProS on newly differentiated DCs (i.e., at day 0). MerTK is shown in green, ProS in magenta. Orange arrows indicate white spots in which both proteins clearly colocalize. The red arrow indicates the flattest part of the cell where the apical membrane is in focus. In these areas, ProS is not observed. (**B**) Zoomed in on the nuclear area of a different dual colour confocal image, and overlaid with a bright field image to highlight the nucleus and its surrounding envelope (oval shaped structure with clear boundary consisting of a very bright and then a very dark layer). Orange arrows indicate spots of MerTK-ProS colocalization that are associated to the nuclear envelope. Cells are minimally permeabilized in order to clearly see the fluorescent spots at the nuclear envelope (NE). (**C**) Quantification of colocalization using the Pearson correlation coefficient (ImageJ, coloc2) in the case of the membrane and cytoplasm, and by visual inspection for the NE. Both methods give a comparable degree of correlation between 0 and 1. Areas with the apical membrane in focus were chosen for the membrane portion of the analysis (membr), the rest of the cell body excluding the nucleus was categorized as the cytoplasm (cyto). On zoom-in images like the ones shown in B, we manually counted the percentage of MerTK spots at the NE that colocalize with ProS. Data of 2 different donors was pooled, each with around 10-20 cells imaged and analysed.

Focusing on different cellular areas in more detail, it appears that colocalization is mainly observed in the perinuclear area, while at the cell periphery, which consists mostly of the plasma membrane, MerTK is mainly observed alone (red arrow). This suggests that MerTK internalization immediately follows upon ProS binding in such a way that MerTK-ProS complexes are rarely observed at the membrane level. At the level of the nuclear envelope, we were able to observe multiple receptor-ligand complexes already associated to the nuclear envelope (NE) (orange arrows in Fig. II.7 B). To quantify the colocalization between MerTK and ligand ProS as a function of the different sub-cellular regions, we separated the images into periphery (mainly the membrane), cytoplasm and NE bound. The degree of colocalization clearly increases as the MerTK-ProS complexes move towards the nuclear region (Fig. II.7 C), indicating that ProS binding is a requirement for nuclear MerTK translocation.

Connecting our observation of highly increased translocation of MerTK during day 0 of culture versus day 4 to the potential role of ProS in driving this process, we

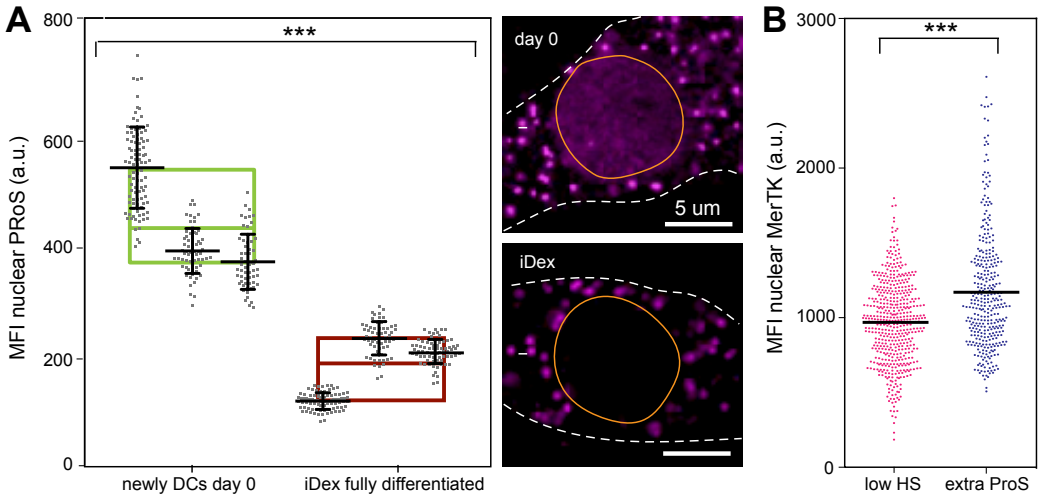

Figure II.8: The effect of ligand ProS binding on nuclear translocation of MerTK (**A**) MFI of nuclear ProS at day 0 and after differentiation into iDexs. Each spot represents a single nucleus; small plots in larger bars represent the 3 different donors measured. Statistics was performed using the average value of each donor. Side panels provide a representative fluorescence image of ProS at both time points. The dotted line indicates the cell boundary, and the orange line the nuclear envelope. (**B**) MFI of nuclear MerTK with and without the addition of extra recombinant human ProS during culture. Monocytes were cultured normally up to day 0. Then, they were differentiated into iDex DCs using cytokines and Dex, but using a lower concentration of HS (1% instead of 10%). This percentage was experimentally determined as the lowest concentration at which the DCs still developed normally (assessed visually). During the last 48h of differentiation, recombinant human ProS was added to one of the conditions (concentration according to Cabezón et al.[10]). Data from 3 different donors was pooled.

hypothesized that more ProS would be found in the nucleus at day 0 than at day 4. We thus quantified the amount of nuclear ProS in day 0 and iDex DCs, and indeed found that just like for MerTK, there is more than a two-fold increase of ProS in the nucleus at day 0 cells as compared to iDexs (Fig. II.8 A). These results further strengthen the hypothesis that ProS plays an important role in facilitating the trafficking of MerTK. Since dendritic cells require the presence of human serum (HS) in their growth medium, and HS naturally contains high levels of ProS, it was not feasible to fully deprive the cells of ProS to further investigate its direct effect on MerTK translocation. However, we cultured the cells in the presence of a reduced HS concentration, and compared this to cells that were cultured in the same serum conditions but with the extra addition of soluble ProS. A significant increase in the amount of nuclear MerTK was observed when there is more ProS available in the medium (Fig. II.8 B), corroborating our previous results that ligand binding is most likely a key factor in regulating nuclear translocation of MerTK.

MerTK traffics through the ER when being shuttled into the nucleus

We next sought to determine via which cellular route MerTK is translocated into the nucleus. To our knowledge, two major routes have been proposed in the literature for the delivery of surface proteins into the nucleus. The first one describes the role of so-called nuclear envelope-associated endosomes (NAEs) to deliver surface proteins all the way from the membrane to the nucleus[43]. These NAEs are a type of early endosomal vesicles positive for the marker EEA, that are thought to travel the full distance from the membrane to the nucleus, without passing through the Golgi. Once at the nuclear envelope, the vesicles fuse with the NE and release their content into the nucleus. The second route is a reversed version of the pathway that newly synthesized membrane proteins take[37,42]. After endocytosis, the proteins end up in the Golgi and get translocated into the ER via COPI-coated retrograde vesicles[37]. Subsequently, the proteins follow the previously described INTERNET (integral trafficking from the ER to the NE transport) pathway from the ER into the inner nuclear membrane (INM)[42]. Both models however agree on the importance of protein importinβ in targeting the RTK towards the nucleus by binding the NLS (nuclear localization sequence). They also both describe the potential role for translocon Sec61 in the final translocation of the receptor across the INM into the nucleoplasm[42,43].

We first confirmed that intracellular MerTK is indeed not targeted for degradation, which would be expected for an phagocytotic receptor in a more classical view. Dual colour confocal images of both MerTK and the lysosome marker LAMP1 show a very strong anti-localization (Fig. II.9 A), clearly indicating that intracellular MerTK is not located in the late endosomes or lysosomes. To further distinguish whether MerTK gets into the nucleus by NAEs or the INTERNET pathway, we performed dual colour confocal

imaging of MerTK and the typical markers of several intracellular components. To ensure that we are looking at MerTK coming from the membrane and not at newly synthesized MerTK on its way from the Golgi to the membrane, we labelled MerTK either by staining the ligand ProS, or by staining auto-phosphorylated MerTK, a process that only happens upon ligand binding and activation at the membrane level. Figure II.9 B displays both MerTK and NAE marker EEA1 in 2 different colours. We do not find significant colocalization between both proteins, although in rare cases MerTK seems to reside in a EEA1 positive vesicle (zoom-in inset). These results are in line with a model in which initial internalization of MerTK is mediated by early endosomal vesicles and

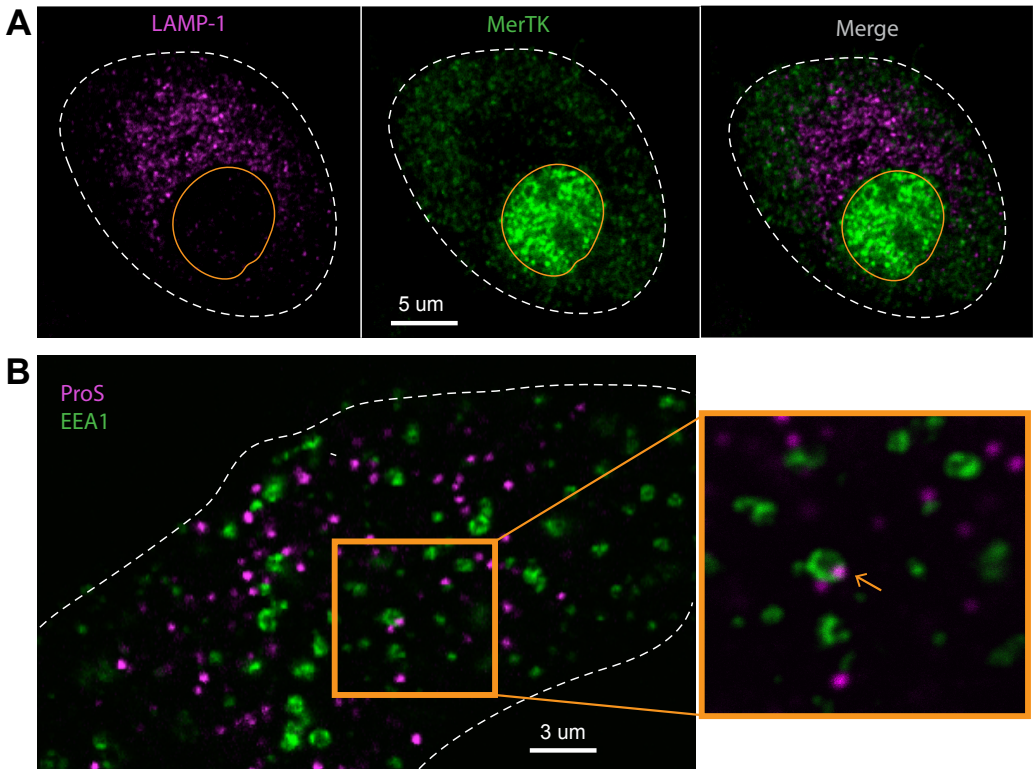

Figure II.9: Identification of intracellular compartments containing MerTK (**A**) Representative dual colour confocal image of MerTK in green and LAMP1 staining the lysosomal compartment in magenta. There is clear antilocalization between both components. The dotted line indicates the cell boundary, and the orange line the nuclear envelope. (**B**) Representative dual colour confocal image stained with αPROS1 visualizing internalized MerTK and EEA1 visualizing early endosomal vesicles. Colocalization is observed only in 1 vesicle, indicated with the orange arrow in the inset.

later taken over by another component (INTERNET-model), rather than a model in which EEA1 positive vesicles are the main MerTK transporting factor all the way towards the nuclear membrane (NAE-model).

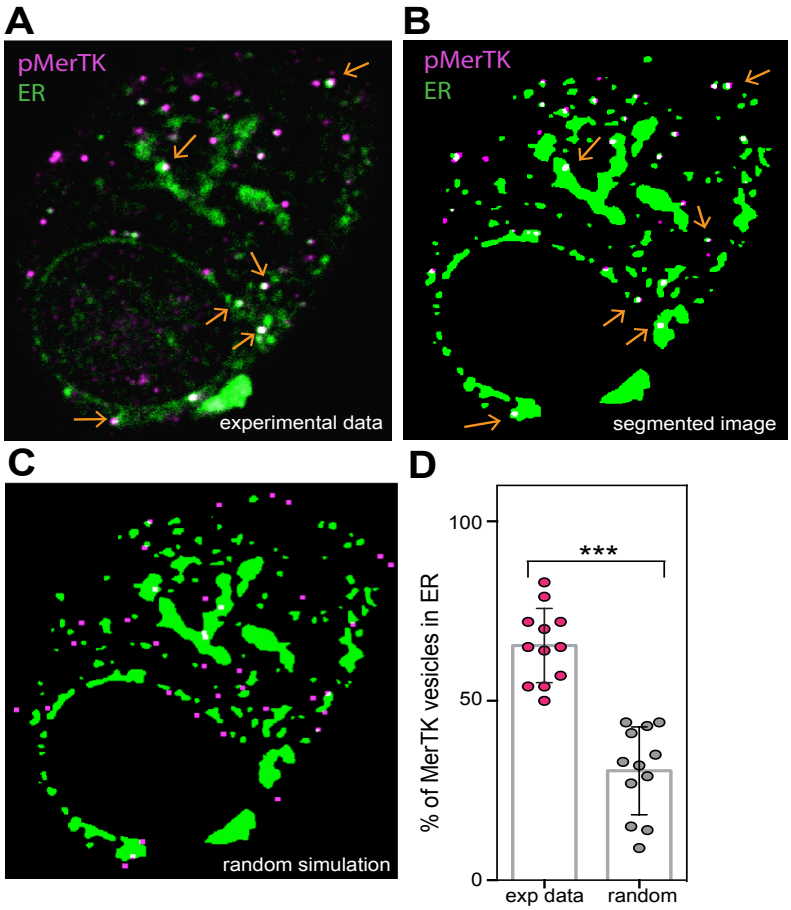

Figure II.10: MerTK in the ER (**A**) Representative dual colour confocal image of auto-phosphorylated MerTK (auto-phosphorylation happens at the membrane upon ligand binding) and the ER marked by calreticulin. Orange arrows indicate clear sport in which both components colocalize. (**B**) Segmented image of A, using the software of Rizk et al.[62], resulting in a binary image for both colours. (**C**) Binary image of the ER, overlaid with a simulated image of random MerTK distribution. The same number of MerTK vesicles as in B are randomly distributed over the intracellular area excluding the nucleus. (**D**) Degree of colocalization in binary images for the experimental images and for randomly simulated distribution of MerTK. Colocalization was considered positive when at least half of the pixels of the MerTK vesicle colocalized with the ER. Data from 2 different donors (6 cells each) was pooled.

To further support the INTERNET-model, we performed dual colour confocal imaging of MerTK and the ER, stained for its common marker calreticulin (Fig. II.10 A). A clear colocalization between both components (orange arrows) is observed throughout the cell body. However, since the ER covers a large part of the cell, a certain degree of colocalization is expected to occur even when there is no real association between both components. We therefore generated *in silico* images with a random distribution of $MerTK^+$ vesicles over the cell area, excluding the nucleus, and segmented images (segmented according to Rizk et al.[62], Fig. II.10 B) of the ER creating a clear mask of ER-positive and ER-negative areas. Overlaying these 2 generated images results in a much lower degree of colocalization than that observed experimentally (Fig. II.10 C,D). This demonstrated that there is a real association between MerTK and the ER that deviates from a random distribution, favouring the INTERNET-model over the NAE-model. Based on these results, we suggest that MerTK is most likely being translocated into the nucleus via retrograde trafficking through the ER and subsequently to the outer and inner nuclear membrane to finally be released inside the nucleoplasm. A similar pathway has been described for the nuclear EGF receptor[42].

The endocytic receptor LRP-1 facilitates nuclear translocation of MerTK

We have shown that MerTK expression is upregulated at two different stages during the differentiation of monocytes into iDex cells; first, at day 0 when it is almost exclusively found in the nucleus (Fig. II.5 A) and second, on fully differentiated iDex cells where the receptor is mostly membrane associated (Fig. II.1 A and [10]). This opens up the intriguing question as to which parameters determine the final subcellular destination of MerTK in DCs. We showed previously that binding of ligand ProS is a factor in regulating nuclear translocation of MerTK, but since serum levels of ProS are constant in all cases, the availability of the ligand is not a likely candidate to determine the spatial faith of the receptor. We therefore hypothesized that MerTK might require an additional facilitating factor that helps with its shuttling towards the nucleus, and that this factor is probably lacking in fully differentiated iDex cells, where MerTK remains largely membrane associated. An interesting candidate for this purpose is the endocytic receptor LRP-1. This fellow membrane receptor has been shown to form a complex with Axl in order to facilitate internalization[68]. Axl and MerTK are very close relatives within the TAM family, making it conceivable that MerTK and LRP-1 can interact in the same way. Furthermore, LRP-1 has been reported to play a role in the shuttling of soluble environmental factors into the nucleus[43].

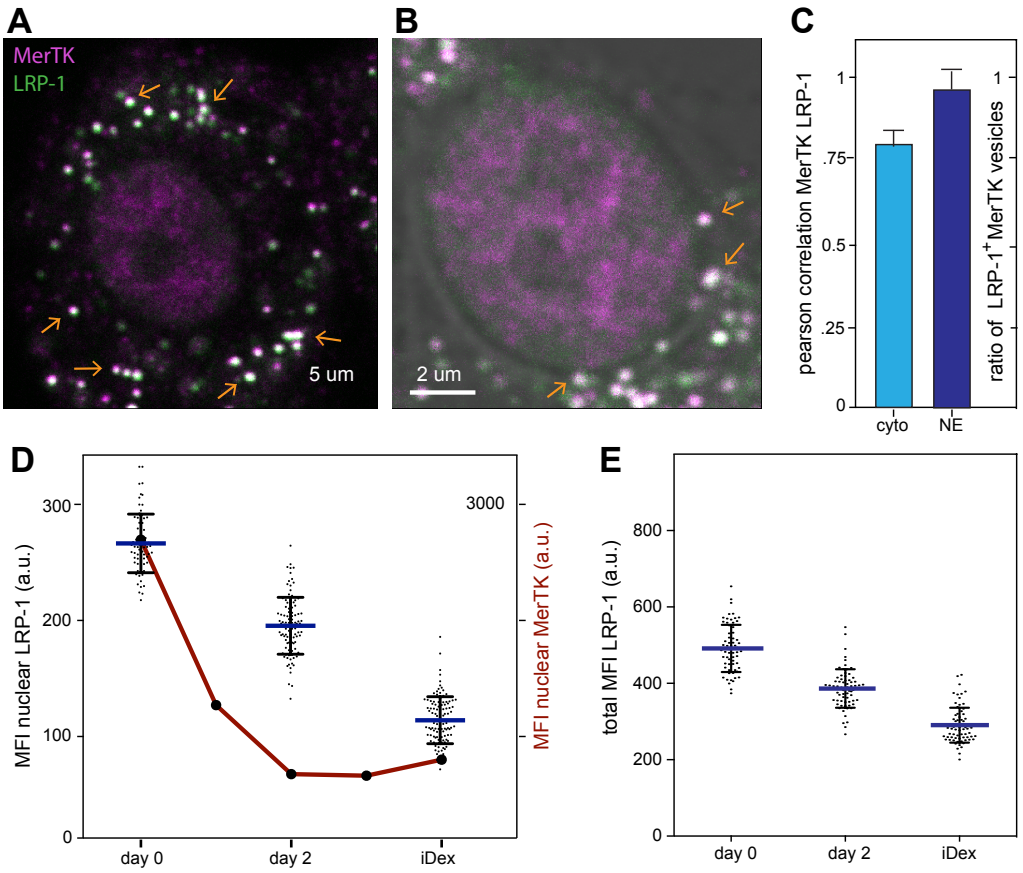

Figure II.11: LRP-1 expression during DC differentiation and its intracellular colocalization with MerTK (**A**) Representative dual colour confocal image of MerTK (magenta) and LRP-1 (green) intracellularly. Orange arrows point to spots of clear colocalization between both receptors. (**B**) Representative dual colour confocal image of MerTK (magenta) and LRP-1 (green), zoomed in on the nuclear area and overlaid with a bright field image to highlight the nucleus and its surrounding envelope (oval shaped structure with clear boundary consisting of a very bright and then a very dark layer). Orange arrows indicate spots in which MerTK and LRP-1 are colocalized, and that are at the same time associated to the nuclear envelope, crossing the nuclear border. (**C**) Quantification of the degree of colocalization between MerTK and LRP-1, both intracellularly and at the nuclear envelope. The Pearson correlation coefficient was used in the first case, and determined using Coloc2 in ImageJ. Data of 3 different donors was pooled. For the NE, colocalization was visually determined for each vesicle found. (**D**) MFI of nuclear LRP-1 over time in culture, at day 0, day 2 and iDexs (= day 4). The red curve together with the right y-axis represents the same data for MerTK to facilitate comparison. Data of 3 donors was pooled. (**E**) MFI of LRP-1 in the entire cell (membrane (which did not exceed isotype control levels) + cytosol + nucleus) over time in culture, at day 0, day 2 and iDexs (= day 4). Data of 3 donors was pooled.

To elucidate whether LRP-1 plays a similar shuttling role for MerTK, we performed dual colour confocal imaging of both MerTK and LRP-1 to investigate their interaction in DCs. An extremely strong colocalization between both receptors intracellularly became readily apparent (Fig. II.11 A). This colocalization is even more clearly observed at the level of the NE, where multiple receptor complexes already associate to the NE (orange arrows in Fig. II.5 B). We quantified the degree of colocalization by determining the Pearson correlation coefficient between both receptor over many images, confirming a strikingly strong intracellular colocalization between MerTK and LRP-1 (Fig. II.11 C).

To investigate whether the amount of nuclear LRP-1 changes as a function of DC differentiation just like the amount of MerTK does, we quantified the amount of nuclear LRP-1 in day 0, day 2 and iDex DCs (Fig. II.11 D). Comparing the changes in expression of LRP-1 to that of MerTK over time clearly shows that both receptors follow the same trend during DC maturation. However, unlike MerTK whose expression increases again towards the final stage of differentiation when most of the receptor is membrane associated (i.e., at day 4), the total expression levels of LRP-1 remain low at this same stage (Fig. II.11 E). These results make it conceivable that LRP-1 plays an important role in regulating the sub-cellular partitioning of MerTK by tuning the degree of MerTK that is translocated to the nucleus, versus the amount of receptor that remains at the membrane.

In a model in which LRP-1 acts as a chaperone in bringing MerTK from the membrane to the nucleus, one would expect to find a correlation between the expression levels of both proteins in the nucleus. Taking advantage of naturally occurring cell-to-cell variability, we were able to demonstrate that the more nuclear LRP-1 a cell has, the more nuclear MerTK it has as well (Fig. II.12 A). This indicates a direct correlation between the translocation of both receptors. To show that it is indeed MerTK that is chaperoned by LRP-1 and not the other way around, we chemically stimulated nuclear translocation of LRP-1 by adding one of its many ligands RAP in the medium (Fig. II.12 B). Stimulating LRP-1 translocation directly leads to an increased translocation of MerTK (Fig. II.12 C), again pointing towards a facilitating role of LRP-1 in the shuttling of MerTK into the nucleus. Our results thus strongly implicate a direct role for LRP-1 in the partitioning of MerTK over either the membrane or the nucleus, regulating its spatial faith by acting as a chaperone molecule.

Nuclear MerTK is associated to chromatin

After identifying how and upon which stimuli MerTK reaches the nucleus, we sought to get further insight in its nuclear function. Other groups have identified various roles for

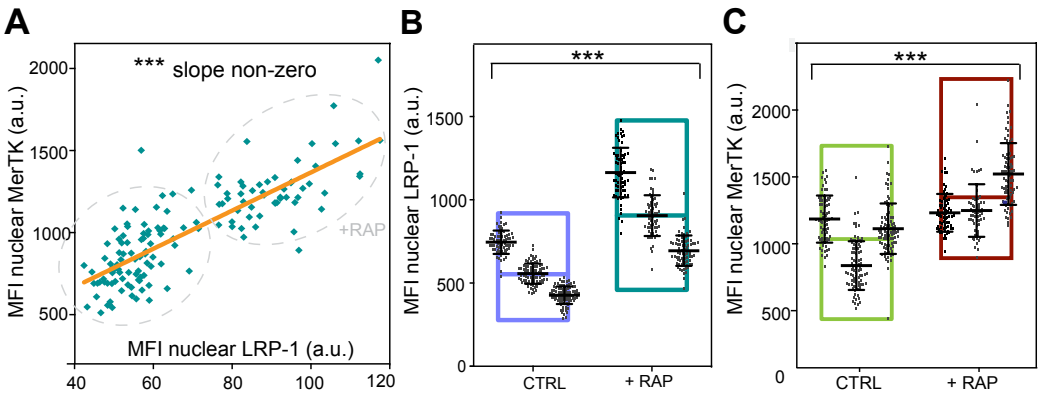

Figure II.12: The role of endocytic receptor LRP-1 in nuclear translocation of MerTK (A) Correlation between the nuclear MFI of both MerTK and LRP-1 at the single cell level. The slope significantly deviates from zero, indicating a positive correlation. Data from cells with and without the addition of RAP (a ligand of LRP-1) are included, visible in the two clouds of data points indicated by the grey dotted ovals. **(B)** MFI of nuclear LRP-1 with and without the addition of RAP, a ligand of LRP-1, to the culture. Monocytes were isolated normally, and RAP was added to one of the cultures after a few hours up to day 0, when the cells were harvested for imaging. **(C)** MFI of nuclear MerTK with and without the addition of RAP to the culture. Monocytes were isolated normally, and RAP was added to one of the cultures after a few hours up to day 0, when the cells were harvested for imaging. A-C Each spot represents a single nucleus; small plots in larger bars represent the 3 different donors measured. Statistics was performed using the average value of each donor.

RTKs in the nucleus, including DNA repair[50], transcription[39,48] and replication[49]. A previous study in Jurkat T cells showed that nuclear MerTK is partially soluble and partially bound to chromatin [46]. We thus hypothesized that MerTK in DCs must also be, at least partially, associated to chromatin in order to carry out one of these aforementioned functions. We first verified chromatin association using an ensemble technique in which we separated the DCs in different cellular fractions: the cytoplasm, the soluble part inside the nucleus and the chromatin bound fraction[57]. These fractions were subsequently run on a western blot, and stained for MerTK. Similarly to Jurkat T cells[46], we find that MerTK is present in all three fractions in both DCs and DC-like THP-1 cells, including in the chromatin bound fraction (Fig. II.13). Thus, it is conceivable that nuclear MerTK indeed plays a role in genome regulation.

To more precisely determine the type of genome regulation that MerTK is involved in, we then attempted to perform ChIP-Seq (chromatin immunoprecipitation sequencing) profiling experiments to identify genomic regions influenced by MerTK, as well as

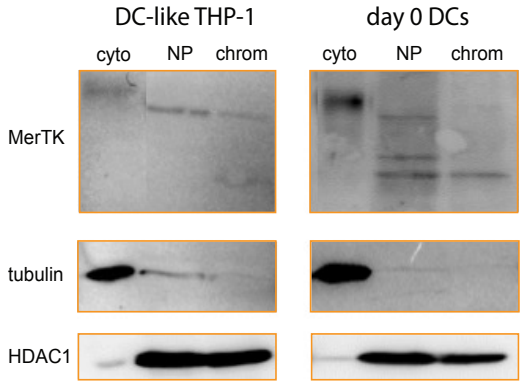

Figure II.13: MerTK in different cellular fractions. Representative western blot showing the relative abundance of MerTK in different cellular fractions (cytoplasm, nucleoplasm, chromatin bound) in both DC-like THP-1 as well as day 0 DCs. Tubulin (cytoplasmic marker) and HDAC1 (nuclear marker) staining indicate a proper fractionation of the cells.

nuclear IP of MerTK followed by quantitative mass spectroscopy to pinpoint the nuclear factors that MerTK forms a complex with. The fact that no validated MerTK antibody exists for these techniques, together with the enormous demand of cellular material that is incompatible with the isolation and culturing of monocyte derived DCs however made this task too challenging, regrettably leaving this question unaddressed.

To get a first insight in the spatial relationship between MerTK and chromatin at the molecular level, we imaged both components simultaneously using dual colour STORM (stochastic optical reconstruction microscopy) microscopy following the approach of Ricci et al[60] (Fig. II.14). This super-resolution technique provides nm resolution capable of identifying individual fluorescently labelling MerTK and histone molecules within the crowded environment of the nucleus with a localization precision of about 20nm (see also Part I of this thesis for a more extensive explanation of the technique). Figure II.15 A displays such a representative dual colour reconstructed STORM image of MerTK and the histones. In mammalian cells, the nuclear periphery is enriched in condensed heterochromatin, generally associated with transcriptional repression[69]. Several studies have demonstrated a direct link between the association of chromatin to the nuclear lamina and gene silencing[70–74]. In our images, the condensed heterochromatin is clearly visible as a dense ring at the edge of the nucleus. This ring is almost completely devoid of MerTK (Fig. II.15 A upper right panel). In the central area of the nucleus where the chromatin is much less dense, a strong MerTK signal is observed (Fig. II.15 A lower right panel). In this area, we clearly resolved elongated structures with both molecules present (grey dotted line) that resemble a configuration in which the nucleosomes are well separated, DNA occupancy is low and the chromatin is accessible[60]. The strong localization of MerTK to areas in which the DNA is in an accessible configuration and its clear exclusion from the dense heterochromatin suggests that MerTK interacts with active genomic regions.

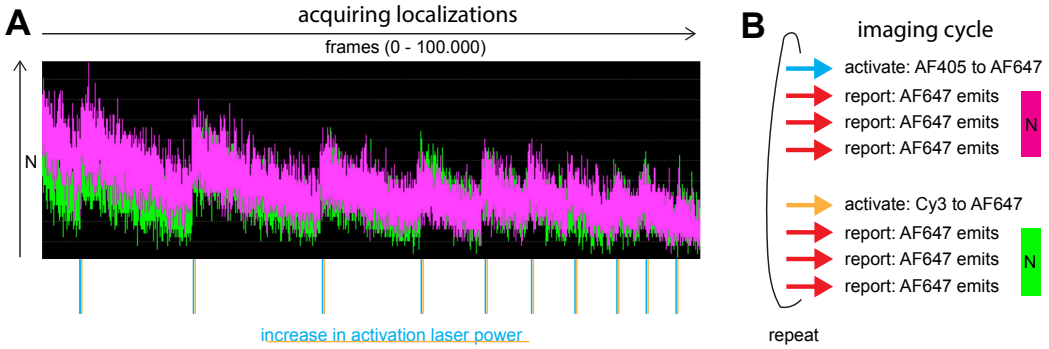

Figure II.14: Dual colour STORM imaging strategy. (**A**) Representative imaging trace during STORM acquisition. The time expressed in number of frames acquired is plotted against the number of localizations identified per frame. The blue/orange lines indicate when the activation laser power was increased, which is clearly seen in the peak increase in localizations registered. Over time though, the number of localizations is progressively going down, indicating exhaustive imaging of all fluorophores. The traces also show that the number of localizations for both colours (MerTK in magenta and panHis in green) are comparable, justifying used 2-color imaging approach with minimal risk for bleed through. (**B**) Schematic representation of the excitation and readout fluorescence in STORM. First, AF405 staining MerTK is excited by a pulse of the 405 nm laser line, which activates the attached reporter dye AF647. Then, 3 pulses of the 647 nm laser line force the emission of photons from AF647, and puts the dye back into the dark state, until after the last pulse no localizations are recorded anymore. This makes the way free to start imaging the next colour without crosstalk. Cy3 staining panHis is excited by a pulse of the 561 nm laser line, and activates the attached reporter dye AF647. Then, 3 pulses of the 647 nm laser line force the emission of photons from AF647, and puts the dye back into the dark state, ready for the next imaging cycle.

We then quantified the interaction between MerTK and euchromatin (Fig. II.15 B). This was done by manually selecting areas in the centre of the nucleus in reconstructed dual colour STORM images (Fig. II.15 C), avoiding the dense histone ring at the periphery as well as the nucleoli. In these areas, the Mander's overlap coefficient between both colours was calculated to determine their degree of colocalization. This was images of randomly distributed MerTK at the same density. A strong colocalization is compared to the degree of colocalization between histones and *in silico* generated observed both in day 0 DCs as well as in iDex cells. This large colocalization significantly deviated from randomly expected colocalization between both proteins at the same density level (Fig. II.15 B) demonstrating that MerTK localizes in regions where chromatin is accessible and strongly suggesting its involvement in genome regulation.

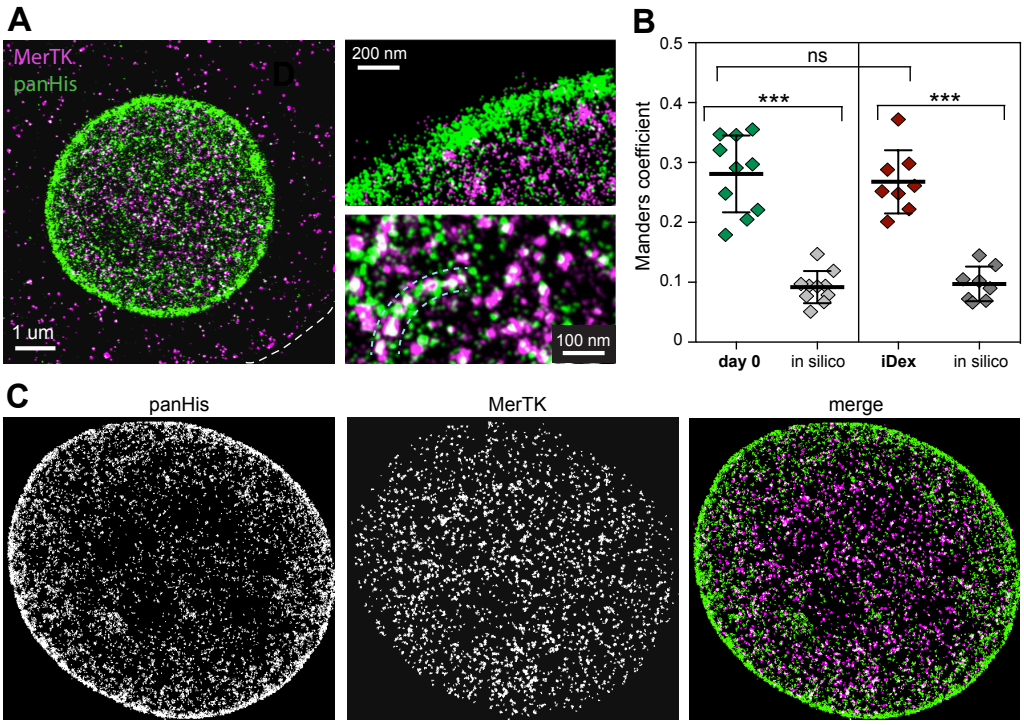

Figure II.15: Dual-colour STORM imaging reveals a spatial relationship of MerTK with chromatin. (**A**) Representative reconstructed dual colour STORM image of MerTK and panHis in the nucleus of a day 0 DC. The nucleus is delineated by a dense ring of histones (the heterochromatin) that is virtually devoid of MerTK. The dotted white line indicates the cell boundary. The zoom- in panels show clear colocalization between the chromatin and MerTK, and show typical elongated structured (dotted grey lines). (**B**) Quantification of the colocalization between panHis and MerTK) using the Manders overlap coefficient. The degree of colocalization was determined at day 0 DCs as well as in iDex. In both cases the experimental data was compared to the colocalization between panHis and *in silico* generated images in which the MerTK clusters were randomly distributed over the nuclear area. Data from 2 different donors was pooled. (**C**) Pixelated binary reconstructed STORM images of both panHis and MerTK, and the merge of both channels. Pixel size corresponds to the position accuracy, namely 20 nm. These binary images are used to calculate the colocalization between both colours. Binary pixelated images are required for this correlation analysis since raw localizations with exact *x,y* positions will never perfectly colocalize and are therefore not suitable for determining the degree of colocalization between MerTK and panHis.

To confirm that the observed colocalization is not a result of cross talk during the imaging process and/or cross-reactivity of the antibodies, we focused on areas where signal from only one of the two proteins is expected to be found: cytosolic vesicles in the case of MerTK (Fig II.16 A) and the heterochromatin ring in the case of the histones (Fig II.16

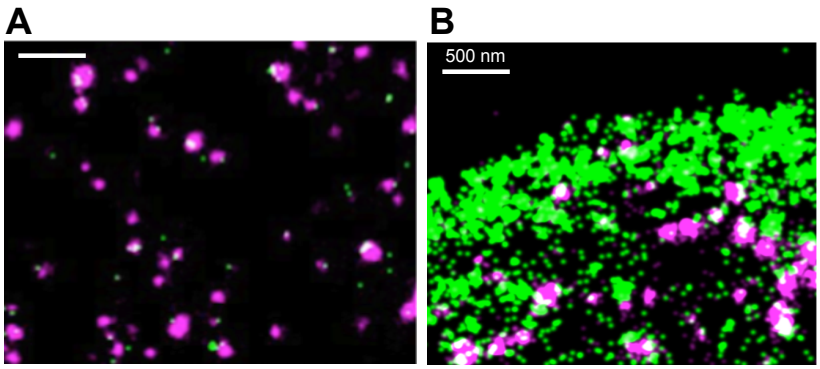

Figure II.16: Bleed-through is very low in our dual-colour STORM images. (**A**) Representative reconstructed STORM image of a cytosolic area in which mainly MerTK (magenta) is present and barely any signal from panHis (green) is observed. MerTK vesicles show exclusively fluorescence arising from the AF405/AF647 dye pair (only 2% of crosstalk). (**B**) Representative reconstructed STORM image zooming in on the nuclear periphery where we find a pure panHis signal (green) coming from the Cy3/AF647 dye pair.

B). Indeed, a very clean one colour signal was collected in both cases with a bleed through of less than 2%. These results thus further strengthen the hypothesis that MerTK interacts with euchromatin.

We have previously shown that nuclear MerTK levels are higher in day 0 DCs than in fully differentiated iDex cells (Fig. II.5 B). Taking advantage of the higher resolution provided by STORM, we quantified the number of localizations in each fluorescent spot as well as the density of MerTK spots in nuclear regions. The large number of localizations in each spot are a clear signature of the formation of MerTK clusters[60]. Our results

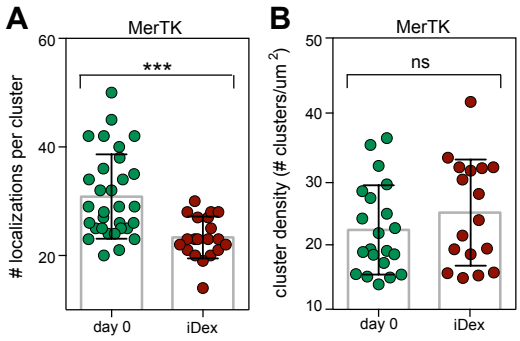

Figure II.17: Degree of MerTK clustering in the nucleus. (**A**) Quantification of the number of localizations per MerTK cluster in the nucleus of both day 0 DCs and for iDex DCs. The data was obtained from dual colour STORM images, exclusively focusing on the MerTK staining. Data from 3 different donors was pooled. The average value per cell is represented. (**B**) MerTK cluster density, i.e., the number of clusters per μm^2. No significant difference is detected between day 0 DCs and iDex DC.

clearly show that MerTK arranges as dense clusters on day 0 DCs, containing a larger number of molecules as compared to iDex cells (Fig. II.17 A). Interestingly, the cluster density is similar to both cell types (Fig. II.17 B), indicating that the difference in the levels of MerTK in day 0 DCs and iDex observed by confocal microscopy are mostly due to an increased clustering of MerTK on day 0 DCs. Moreover, this increased clustering might correspond to more potent functional units.

A recent super-resolution study with STORM showed a direct correlation between the differentiation state of a cell and the degree of chromatin compaction super-resolution microscopy[60]. By mapping the organization of histone H2B in the nucleus of different cell types, the authors discovered that the more differentiated the cells were, the less open and accessible their chromatin was. Based on this work we hypothesized that newly DCs at day 0 might hold their histones in a more open conformation as compared to fully differentiated iDexs at day 4. To investigate this possibility, we stained histone H2B in both cell types and carefully compared the degree of compaction following the approach of Ricci et al[60]. Reconstructed images were first generated from the raw STORM data (Fig. II.18 A) in order to create a density map of the H2B signal and finally grouped the individual STORM localizations into clusters (Fig. II.18 B). The average number of localizations per cluster and the cluster density (number of clusters per um^2) were then calculated to estimate the degree of chromatin compaction. The data show a clear increase in the number of H2B localizations per cluster (Fig. II.18 C) as well as density (Fig II.18 D) on cells that have been fully differentiated into iDexs. An increase in both parameters at the same time interestingly suggests that fully differentiated DCs have more histones covering their DNA. We confirmed this using traditional wide-field imaging, in which we show an increase of 30% in histone expression levels in the nucleus of iDex cells (Fig. II.18 E). This is in line with previous work where a similar increase in the total histone content was reported between pluripotent and differentiated cells[75]. An additional study showed that the histone quantity in monocytic derived DCs, similar to the ones we used in our studies, can indeed vary significantly upon treatment with different immunological stimuli[75]. As H2B is directly involved in DNA compaction, these results thus reveal that chromatin is indeed in a more accessible conformation during early stages of DC differentiation, i.e., at day 0 DCs. Our observations that MerTK shows increased clustering and preferentially interacts with chromatin exactly during this genomically active stage, together with its tendency to associate to euchromatin rather than to heterochromatin strongly points towards a role for nuclear MerTK as a transcription factor during DC differentiation.

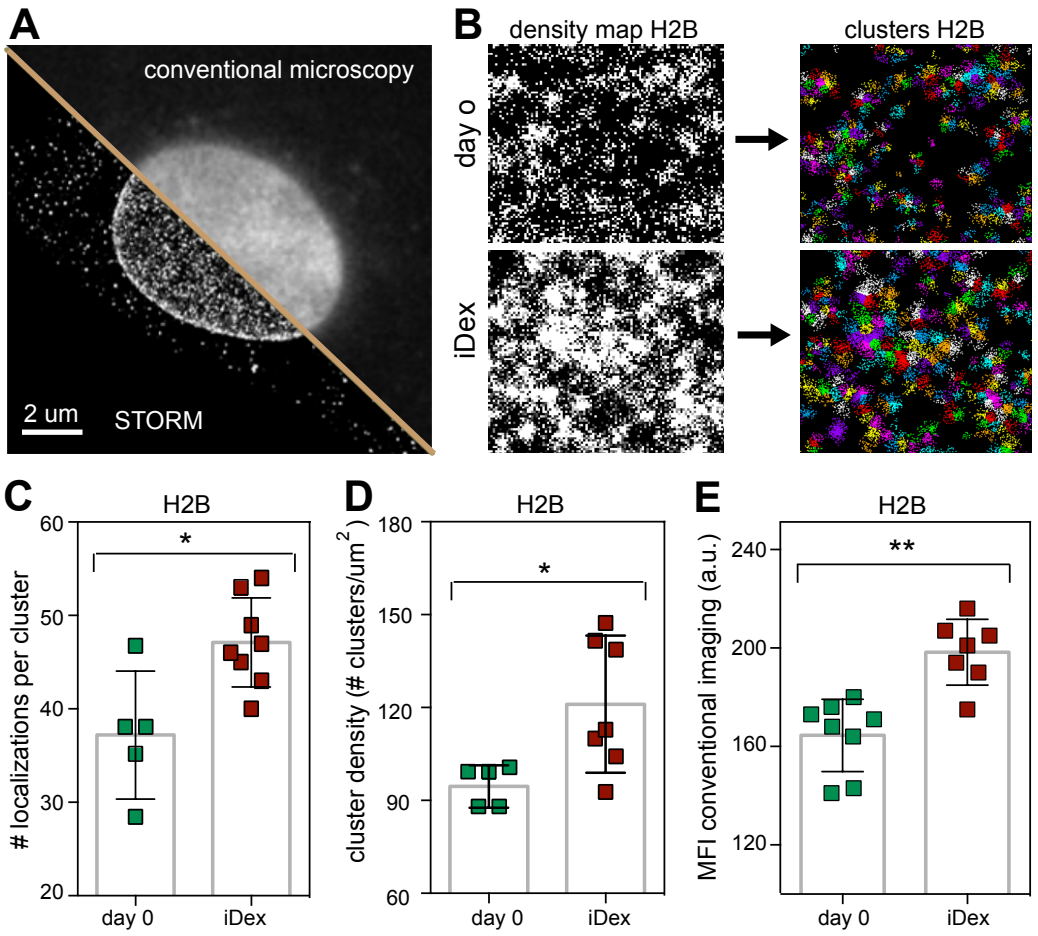

Figure II.18: Chromatin compaction as a function of DC differentiation. (**A**) Representative single colour reconstructed STORM image of H2B in the nucleus of a day 0 DC. The image was partially overlaid with a conventional image of H2B in the same cell to show the increase in resolution gained by using super resolution STORM imaging. (**B**) Image processing approach to generated density maps of the H2B signal (left) and classification of clusters according to the number of localizations (right), following the approach of Ricci et al.[60]. (**C**) Quantification of the number of localization per H2B cluster in day 0 and in iDex DCs. (**D**) Quantification of the H2B cluster density (the number of clusters per μm^2) in day 0 and in iDex DCs. (**E**) MFI of nuclear H2B in day 0 vs iDex DCs in confocal images. Conventional images were taken before STORM acquisition of the same cells. This shows together with C and D that the global increase in localizations per cluster and cluster density is also reflected by a total increase of expression levels of H2B in the nucleus of around 30%. Each symbol in plots C-D represents an average value per cell imaged.

II.5 Discussion

In this thesis we have for the first time, to our knowledge, characterized the spatial distribution of MerTK on the plasma membrane of tolerogenic DCs at the nanometre scale using super-resolution microscopy. We found that the receptor organizes in small nanoclusters on the plasma membrane of human DCs. Moreover, we identified a pool of intracellular MerTK that is mainly located in the nucleus, regardless of whether the DCs have a tolerogenic or immunogenic phenotype. The degree of nuclear localization strictly depends on DC maturation, uniquely indicating a physiological function for the nuclear translocation of a RTK in the context of immunity. We subsequently found that the nuclear translocation of MerTK is ligand dependent, and that its trafficking into the nucleus proceeds through the ER. The endocytic receptor LRP-1 was identified as a chaperone in this process, implicating for the first time a role for this receptor in RTK translocation. We finally characterized the nanoscale spatial relationship between MerTK and chromatin within the nucleus of intact DCs using super-resolution microscopy. Our data suggest that nuclear MerTK interacts with transcriptionally active genomic regions, possibly functioning as a transcription factor that regulates the differentiation of dendritic cells.

MerTK nanoclustering on the plasma membrane of tolerogenic DCs

The organization of immunoreceptors in nanoclusters is a very well established phenomenon[52–55,76–79]. Nanoclustering of membrane receptors is thought to facilitate their effective ligand-binding affinity to multivalent ligands[53,80]. For single ligands, nanoclustering of the receptor can also offers an affinity advantage, particularly in the case of low binding affinities, since rapid rebinding upon disengagement to another receptor in close proximity is promoted[81]. In our super-resolution STED experiments, we observed that MerTK forms small nanoclusters on the surface of tolerogenic DCs composed by an average of three molecules per nanocluster (Fig. II.1 C). Given the fact that membrane MerTK is highly expressed on tolerogenic DCs, we initially hypothesized that MerTK nanoclustering would play a similar role of increasing ligand affinity when these tolerogenic DCs bind to T-cells to execute their suppressive function[10]. We therefore promoted the interaction between mature tolerogenic DCs (tolDCs) and either T-cell markers deposited on glass or to full T-cells, to get more insight into the surface distribution of MerTK within the immunological synapse. For the first type of experiments, we used microcontact printing (μCP) to stamp immunological synapse marker ICAM-1 and anti-MHC-II antibodies to bind and activate MHCII in squared patterns on a glass cover slip, following a previously established protocol[82] also described

in Part I of this thesis. Previous studies using lipid bilayers demonstrated that engagement of MHCII and adhesion through ICAM-1/LFA-1 is indeed sufficient to induce a functional immunological synapse[83]. Interestingly, we observed that MerTK surface distribution is completely independent of the printed proteins as seen from the lack of MerTK accumulation to the positive squares (Fig. II.19 A). This lack of MerTK accumulation is not due to a failure of the tolDC to recognize the printed proteins, since ICAM-1's counter molecule LFA-1 does indeed accumulate to the positively stamped areas (Fig. II.19 B). We furthermore promoted tolDCs to interact with isolated $CD4^+$ T-cells in solution in the presence of superantigen.

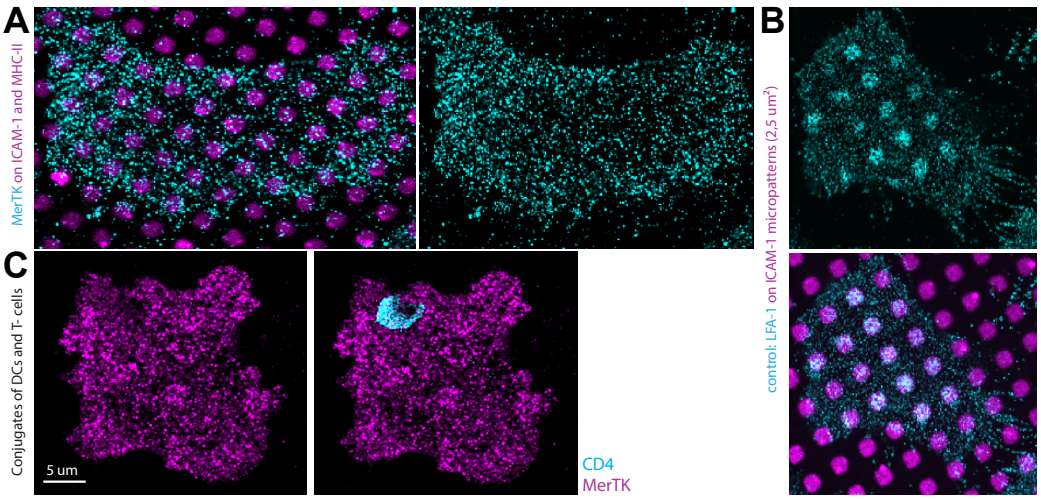

Figure II.19: MerTK distribution in the immunological synapse. (**A**) Representative image of a tolDC (iDex DC that underwent 48h of maturation in the presence of IL-1β, IL-6, TNF-α and PGE_2 following established protocol[84]) seeded on a patterned surface. The patterned surface consists of small squares (magenta), 2,5x2.5 µm in size, covered with both ICAM-1 and anti-MHC-II antibodies. The squares are stamped onto a glass coverslip using microcontact printing[82]. MerTK on the membrane of the tolDC is staining (cyan). No specific pattern in the MerTK distribution relative to the patterns is observed. (**B**) As in A, but squares only consist of ICAM-1 proteins and LFA-1 in now labelled on the surface of the tolDC. Clear accumulation of LFA-1 to the ICAM-1 patterns is observed. (**C**) Representative image of a tolDC interacting with a T-cell (cyan, CD4). MerTK on the membrane of the tolDC is stained, and no specific accumulation to the site of T-cell binding is observed.

However even in this more physiological case, no specific accumulation of MerTK to the site of T-cell binding was observed in any of our attempts (Fig. II.19 C). This suggests that MerTK does not directly bind to any ligand on the membrane on the T-cell, but instead executes its tolerogenic effect in a different way. Although these results were initially unexpected, they are fully in line with those reported by Cabezon at al.[10] and

Carrera-Silva et al.[17], where the authors proposed an alternative mechanism of action for tolerogenic MerTK. Activated T-cells produce soluble ProS, which then further activates the same T-cell in an autocrine fashion. However, MerTK on DCs competes with the T-cell for ProS binding. Since MerTK is highly upregulated on the surface of tolDCs, these tolerogenic cells strongly compete with the T-cells for the ligand, effectively depriving them from ProS and subsequently suppressing their activation. It is thus in this way that tolDCs have a negative effect on T-cell proliferation and cytokine production, without a direct binding of MerTK to any ligand on the T-cell surface[10,17]. Obviously, the process of efficient ProS scavenging from the local environment by MerTK requires rapid internalization of MerTK-ProS complexes and recycling of MerTK back to the surface to continue the process. This nicely agrees with our dual colour confocal experiments in which we were almost never able to capture MerTK-ProS complexes at the membrane level (Fig. II.7 A) indicating rapid MerTK internalization upon ligand binding.

In the context of MerTK nanoclustering and its functional role on tolerogenic DCs, it is thus tempting to speculate that clustering might provide an advantage for the rapid internalization of MerTK in order to clear the environment of ProS. Having several MerTK-ProS molecules in close proximity of each other could probably be internalized in one single internalization event, lowering the amount of energy and resources needed for ProS clearance. Having to internalize each ProS molecule individually, bound to a single MerTK molecule, would take longer, leaving more soluble ProS behind to activate T-cells (= lower tolerogenic effect). In addition, it is also conceivable that binding and unbinding of ProS to MerTK is rather weak, so that off rates are much faster than internalization. By bringing MerTK together into small nanoclusters, effective ProS-binding via different receptors in close proximity is increased[81], favouring internalization. Moreover, the small number of MerTK molecules involved in each nanocluster (on average 3, ranging between 1 and 11, Fig. II.1 C) would provide an excellent strategy to optimize MerTK resources for efficient ligand scavenging throughout the local cell environment.

Further experiments to investigate whether nanoclustering indeed facilitates internalization would be of high interest. For example, one could induce additional MerTK clustering by adding α-MerTK antibodies to the cell culture or by using μCP approaches, and assess to amount of fluorescently labelled ProS internalized for different fixed periods of time, and compare these results to those obtained on untreated cells. More elegantly and quantitatively, one could follow the dynamics of ProS in a similar experimental strategy using Single Particle Tracking (SPT) approaches. Tracking the mobility of ProS across the membrane until internalization would provide information

about on internalization rates, and also importantly, on the exact physical mechanisms by which this process is initiated. SPT would be more sensitive to small changes in the internalization rate between the different conditions, and/or to small populations of molecules exhibiting accelerated internalization.

The presence of MerTK in the nucleus

The presence of full-length RTKs in the nucleus has been widely reported over the last decade (reviewed in [34,38,63]). These receptors are thought to escape from the lipid bilayer in the inner nuclear membrane (INM). For the EGF receptor, this escape process has been shown to depend on sec61 β[44], which is part of the larger translocon sec61 pore complex. This complex is traditionally involved in inserting newly synthesized transmembrane proteins in to the lipid bilayer of the ER. In order to accomplish this, the complex has an opening towards the lumen where the protein can enter, as well as a lateral opening allowing the subsequent incorporation of the protein into the membrane. The EGFR is proposed to follow this process in a reversed manner, being extracted from the nuclear membrane through the lateral opening, and released in a soluble form inside the nucleus[42,45].

However, the community has been reluctant to accept these observations mainly because it is very counter-intuitive to envision how membrane-bound receptors could be soluble inside the nucleoplasm given that they contain a transmembrane domain that chemically prefers to be surrounded by lipids. Two different models have been proposed to explain nuclear RTKs bypassing this apparent controversy[34]. The first model involves the proteolytic cleavage of the cytoplasmic domain of the receptor, that then is released into the cytoplasm as it lacks the transmembrane domain[85,86]. Even though this model might be the most intuitive, the presence of many full-length receptors in the nucleus[45] argues against this model. For MerTK, the existence of a short soluble protein version solely containing the extracellular domain has been reported previously[14], which might make the presence of its intracellular counterpart conceivable. However, by labelling different domains of the receptor, we present in this thesis compelling evidence that both the intracellular as well as the extracellular domain of MerTK are found in the nucleus. Another study has previously shown the existence of nuclear MerTK in leukemia cell lines[46]. Although merely observed as a curiosity in this publication and not related to a function, immunological or physiological, their results do support our data showing that full-length MerTK is found in the nucleus of immune cells.

The second model proposes the existence of an isoform on certain types of RTKs only lacking the transmembrane domain (TDM), a modification in size that is too small to be

detect by a western blot for a heavily glycosylated protein. This modified RTK is thought to dimerize with an unmodified version of the same protein at the level of the membrane and during nuclear trafficking. This would provide ligand sensitivity and explain its localization at the cell membrane and the membrane of cellular compartments. Such a soluble, almost full-length isoform has been detected for the FGFR2 receptor[87], which has served as evidence to support this model. However, for many of the known RTKs in the nucleus, including MerTK, the existence of such an isoform has never been demonstrated, and for some RTKs the presence of the transmembrane domain in the nucleus has been specifically shown[88]. It remains however conceivable that small modifications to the TMD, for example in length[89] or hydrophobicity[90,91], facilitate soluble nuclear existence. Systematic characterization of the transmembrane domain of nuclear RTKs at the single amino acid level would be needed to gain better insight in this possibility.

Alternatively, it is conceivable that even though not incorporated in the lipid bilayer, the transmembrane domain is still covered by a small amount of lipids in the nucleus. The concept of nuclear lipids has been widely described over the past 2 decades, and the existence of proteolipid complexes has been observed[92–94]. Direct visualization of nuclear RTKs in the nucleus with a lipid-covered TMD remains out of reach with our current imaging approaches, but experiments with fluorescent lipids and proteins with and without modifications to its TMD in solution could provide a proof-of-concept for this idea. Showing how RTKs can be soluble in the nucleus would most likely be key is accomplishing a wide acceptance of this mechanism within the cell biology community.

Nuclear MerTK as a function of DC differentiation

Within the field of transmembrane receptors in the nucleus, the general consensus is that aberrant or overexpression of the protein causes this atypical nuclear translocation, and that the presence of RTKs in the nucleus is related to malignancies. Our results on MerTK are however markedly distinct in several ways: *First*, nuclear MerTK is found in a very high concentration in healthy non-proliferating dendritic cells. *Second*, nuclear localization of MerTK seems to be exclusively reserved for immune cells (DCs and THP-1 in our experiments, and for Jurkat T cells[46]). Indeed, we showed that overexpression of MerTK in other cell types, both with (HEK293) and without (HeLa) endogenous MerTK, does not lead to nuclear accumulation of the receptor. *Third*, the degree of nuclear translocation strictly relates to DC differentiation, a physiological process that is crucial to basic immunity. Our results thus interestingly suggest a physiological, non-malignant role for a RTK in the nucleus. A previous study by Schmahl et al. suggests a similar regulating role for the receptor tyrosine kinase FGF2 in the early stages of Sertoli cell differentiation[95].

The dependence of nuclear MerTK accumulation upon DC differentiation is interesting in itself, but the observation that nuclear MerTK levels sharply peak during early stages independently of tolerogenic treatment is even more captivating. The sharp peak we observed on newly differentiated DCs suggests a critical time-sensitive and well-regulated need for the presence of the receptor in the nucleus, again pointing to an important physiological function. This synchronous increase during early DC differentiation advocates for a role of nuclear MerTK assisting in the process of gene regulation leading to the maturation of monocytes into DCs, a fundamental immunologic process unrelated to tolerogeneity. This process indeed heavily requires the regulation of differentially expressed genes in which timing is crucial. Determining the expression profile of nuclear MerTK during DC differentiation is thus an important first step towards understanding its nuclear function.

The role of ligand binding in nuclear translocation of MerTK

The involvement of ligand binding in the nuclear translocation of RTKs has been reported previously for several receptors[39–42,46], and as such, our results showing that ProS triggers the shuttling of MerTK towards the nucleus are fully in line with this paradigm. Moreover, we observed a direct correlation between the amount of nuclear MerTK and nuclear ProS during DC differentiation while the amount of serum ProS remained constant during this process. This indicates that ProS is indeed a crucial factor in triggering the nuclear translocation of MerTK. Nevertheless and in contrast to these previous reports we were not able to demonstrate a very strong dependence on ligand binding, neither a very fast response (30-60 min[42]) upon addition of the ligand to the medium. We undertook many attempts to visualize this process more directly. We tried to fully deprive the DCs of human serum which contains ligand ProS, to observe a strong reduction in the amount of nuclear MerTK. Unfortunately, the DCs were not healthy without the serum hampering a reliable comparison between conditions. We also attempted to trigger nuclear translocation of MerTK by ligand addition in several cell lines transfected with MerTK, but we never found a non-immune cell line in which MerTK would traffic into the nucleus (Fig. II.4). Finally, we created fluorescent ProS molecules and followed the incorporation of this ligand into living DCs, but the fluorescent ProS molecules were always ending up in the lysosomes instead of binding to MerTK, most likely due to the artificial presence of the fluorescent tag. It thus remains elusive how strongly the nuclear translocation of MerTK depends on the binding of its ligand due to these technical issues.

LRP-1 as a chaperone for MerTK translocation

Low-density lipoprotein receptor-related protein (LRP-1) is a large transmembrane receptor exhibiting both endocytic and signalling functions. With more than 35 identified ligands, this receptor is extremely pleiotropic[96]. Taking all its different activities into account, LRP-1 has been described as a receptor that regulates the protein composition of the plasma membrane, thereby shaping the cell surface[97]. In the context of immunity, LRP-1 regulates the membrane levels of β1 integrins[98,99], CD44[100] and the phagocytic receptor AXL[68] by facilitating their endocytosis. Knock-down or blocking of LRP-1 leads in all cases to accumulation of the receptors at the membrane level. LRP-1 forms molecular complexes with these receptors either by direct[100] or indirect[68] binding, and endocytosis occurs via clathrin coated pits[100]. Measuring the dynamics of β1 integrins in the absence and presence of LRP-1 blocking agents as well as colocalization studies showed that the intracellular trafficking of this receptor is under the direct control of LRP-1. The final destination of the LRP-1 mediated trafficking is however not always the same. Even though lysosomal degradation is the most common target [68,99,100], LRP-1 can also mediate integrin recycling back to the cell surface.

Our results on the role of LRP-1 in the partitioning and regulation of the spatial faith of MerTK can be fully rationalized under the paradigm that LRP-1 controls the composition of the cell membrane. Like the previously mentioned receptors, we found that MerTK strongly colocalizes with LRP-1 intracellularly. Moreover, we found that MerTK accumulates to the cell membrane when LRP-1 expression levels are low, which naturally occurs during the final stages of DC differentiation (day 4). However, while LRP-1 targets many other receptors towards lysosomal degradation or recycling, we show here that this receptor is also involved in nuclear translocation. It was shown previously that LRP-1 can target soluble toxins from the cell environment into the nucleus in a receptor-ligand fashion[43], but to our knowledge LRP-1 has never been implicated in chaperoning other transmembrane proteins towards the nucleus. We thus propose that the subcellular spatial destination of MerTK is tuned/controlled by LRP-1. When DCs express both MerTK and LRP-1 simultaneously, LRP-1 will bind MerTK and will direct it into the nucleus (day 0) via endocytosis. By contrast, in the absence of, or at reduced LRP-1 levels, assistance for nuclear translocation is compromised, and MerTK remains at the surface (day 4). Complex formation between MerTK and LRP-1 is likely to be mediated by RANBP9 as it is the case for complexing of AXL and LRP-1[68], since we observed clear colocalization between MerTK and RANBP9 in intracellular trafficking vesicles (Fig. II.20). Curiously enough, we observed that the addition of the LRP-1 ligand RAP increased nuclear translocation of both LRP-1 and of MerTK as a result thereof. In contrast to our results,

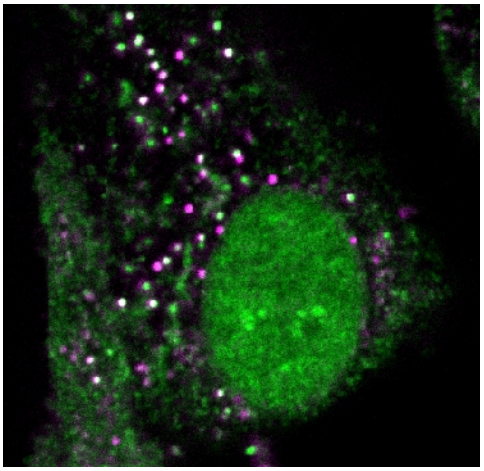

Figure II.20: Colocalization of MerTK and RANBP9 intracellularly. Representative dual colour confocal image of MerTK (magenta) and RANBP9 (green) in a permeabilized iDex cell. Colocalization between MerTK and RANBP9 is observed in intracellular vesicles (white spots). Similar to MerTK, ProS and LRP-1, RANBP9 is also observed in the nucleus of DCs

several studies have used RAP to block LRP-1 induced endocytosis and to retain CD44, AXL and β1 integrins at the cell membrane[68,98,100]. This indicates that LRP-1 association to other receptors is not the only determinant for the spatial destination of the entire complex, but also that the type of ligand bound to LRP-1 influences its chaperoning function, probably in a cell type dependent manner. Further studies are needed to decipher this complex regulating mechanism more extensively, including knock-down experiments of LRP-1 to fully confirm its importance in nuclear translocation. Pinpointing the role of LRP-1 in the process is a great step forward in the molecular understanding of nuclear trafficking since it has never been reported previously. This knowledge can be used to further the understanding of nuclear translocation of other RTKs. Since many other RTKs play an oncogenic role in the nucleus, identifying triggers in this process is of paramount importance for future clinical interference.

Spatial relation between MerTK and chromatin: towards deciphering a nuclear function

Due to the extremely crowed environment in the nucleus and the nanometric size of the chromatin fibres, super-resolution STORM imaging provides an ideal tool to study the organization of the genome with nanometric precision. Several studies have now gained more insight in how our genetic material is stored by either looking at the DNA itself[101,102] or the histones around it[60,103]. All studies so far evidence a clear correlation between shape and functionality: transcriptionally active regions are less densely packed than inactive regions[102] and highly active stem-cells exhibit a more open chromatin configuration than resting somatic cells[60]. These reports on the nanometric organization of chromatin are in

full agreement with studies performed by classical optical microscopy. Indeed, by using more traditional imaging techniques, the nuclear periphery has been already identified as a very large structure that is highly enriched in condensed heterochromatin. Functional studies demonstrated that this highly condensed area is generally associated with transcriptional repression[69]. Furthermore, a direct link between the association of chromatin to the nuclear lamina and gene silencing has been established[70–74]. The clear exclusion of MerTK from this heterochromatin-enriched, condensed genomic region observed in our experiments, together with the strong colocalization observed between MerTK and euchromatin in the central area suggest that MerTK preferentially interacts with active genomic regions. Importantly, by studying the difference in chromatin compaction between DCs in early and active stages *vs* final and resting stages of differentiation we now provide an extra level of functional information. Using super-resolution microscopy, we observed that in the earlier stages of DC differentiation chromatin is more open and, that on fully differentiated DCs chromatin is more compact. Accompanied to these changes in chromatin compaction, we observed a clear increase in nuclear translocation of MerTK on newly differentiated DCs, indicating a role for MerTK at this transcriptionally active phase of differentiation. Given that MerTK preferentially accumulates to transcriptionally active regions, and during a transcriptionally active period in differentiation, it is tempting to speculate that it functions in there as a transcriptional factor regulating DC differentiation.

The analysis presented on our dual colour super-resolution images was performed by simply separating the heterochromatin in the nuclear periphery from the euchromatin in the centre of the nucleus. This separation is however very rough and might not do full justice to the super-resolution data acquired. Alternatively, a more insightful and detailed type of analysis could be done by establishing gradients of chromatin compaction within the nuclear centre and spatially correlating the degree of compaction to the degree of MerTK accumulation. This approach has been actually implemented by Boettinger et al[102] to determine the degree of compaction for different genomic regions. Moreover, using prior knowledge gained from ensemble biochemical tools on the activation state of the same regions, they correlated the degree of compaction to the degree of transcription activation (active, inactive or repressed). Using this established correlation, we should be able to assign whether regions are active or inactive based on the level of chromatin compaction and assign the involvement of MerTK to these regions. However, this experimental approach requires the exclusive labelling of isolated genomic regions using for instance DNA FISH, and STORM imaging in 3D[102]. So far, in our experiments we labelled the entire pool of chromatin, and performed STORM imaged in 2D. This means

that we collected localizations coming from an 800 nm thick slice of the nucleus, and collapsed all the localizations into a 2D image. The neighbouring genomic regions in *x, y* and *z* are therefore all mixed together in our data. When drawing global conclusions about chromatin compaction on different cell types, this effect is averaged out since image reconstruction is performed in a similar way, allowing for faithful comparison amongst different cell types or conditions. However, the results would be less reliable when focusing on smaller regions, which are needed to establish compaction gradients. In this case, obtaining an unbiased correlation between MerTK accumulation and chromatin compaction in small genomic regions becomes challenging. A feasible alternative would be to compare our current dataset with a dataset in which only the active portion of the chromatin is imaged, for example by using a methylation-sensitive antibody or by staining RNApolII. Comparing the degree of MerTK colocalization with chromatin in general *vs* that with active chromatin could provide further insights into its preferential binding at an even higher detail than we currently did.

An additional and very important outcome of our research is that we visualized for the first time the nanoscale organization of chromatin in human dendritic cells using super-resolution imaging. This very general dataset can be of interest for many other studies on dendritic cells. Since we used the same methodology as Ricci et al.[60] for staining, imaging and analysis, we feel confident to directly compare our data to theirs. The authors reported on average 16 localizations per H2B cluster for induced pluripotent stem cells, and around 24 localizations for somatic fibroblasts. In sharp contrast, we found more than a two-fold increase in the number of localizations, with on average 38 localizations per H2B cluster early during DC differentiation, and around 47 localizations per cluster in iDex DCs. These results are extremely appealing since they suggest that chromatin in DCs is very densely packed as compared to fibroblasts and probably, as compared to many other types of cell lines that are frequently used in Cell Biology experiments. This finding might also explain the enormous difficulties we faced in solubilizing the chromatin bound fraction of proteins in DCs (Fig. II.13 and II.21) when using standardized protocols from the Cell Biology community. The results presented in here suggest that in principle, one could classify different cells based on their chromatin compaction. Correlating this to general characteristics and properties of these cells (proliferation, tissue, species, etc.) would ultimately provide novel insights in the functionality of chromatin organization.

MerTK as a transcription factor: how to gain direct functional data?

Other groups have identified various roles for RTKs in the nucleus, including DNA

repair[50], transcription[39,47,48] and replication[49]. Since DCs are non-proliferative cells, a potential role for nuclear MerTK in replication is fully excluded. Its involvement in DNA repair is also not plausible, since there is no reason to expect a specific increase in DNA damage early during DC differentiation when MerTK levels in the nucleus reach peak values. The role of nuclear MerTK acting as a transcription factor is much more probable given the fact that we detected a clear dependence between nuclear accumulation and DC differentiation. The diffuse localization throughout the entire nucleoplasm, but exclusion from both the nuclear envelope as well as the nucleoli are additional elements that advocate for its role as a transcription factor.

Transcription factors are typically characterized by the presence of one or several transactivation domains that are involved in the recruitment of larger multiprotein complexes facilitating transcriptional activity[104,105]. The sequence of these domains is highly conserved and can be predicted based on hydrophobicity and several key amino acids[106,107]. We used an algorithm developed by Piskacek et al. to predict possible 9aaTAD regions in the MerTK sequence, and obtained one domain with a 100% match (Fig. II.21). This strongly supports our proposal that nuclear MerTK acts as a transcription factor during DC differentiation. We are currently undertaking experiments in which this domain is fused to a DNA-binding protein that interacts with a specific luminescent reporter gene. Increased luminescence as a measure of increased transcription upon fusion of the transactivation domain to the DNA-binding protein is expected if the domain indeed contains transactivational functionality. This experimental data is expected to strengthen our claim that nuclear MerTK indeed has the capacity to function as a transcription factor.

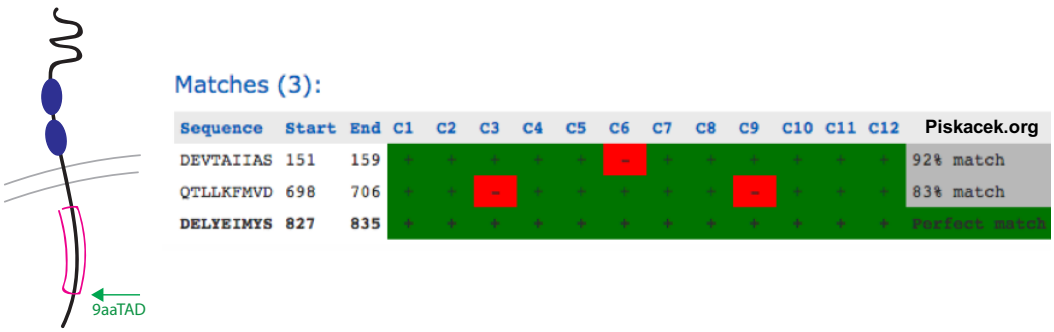

Figure II.21: MerTK contains a predicted 9aaTAD transactivation domain. In silico results obtained from predicting the existence of a 9aaTAD domain with transactivation activity within the MerTK sequence. Results are obtained using the software provided on kiskacek.org using the most stringent conditions. The location of the predicted domain relative to the MerTK protein, at the end kinase domain (depicted in magenta) within the cytoplasmic tail, is indicated on the left.

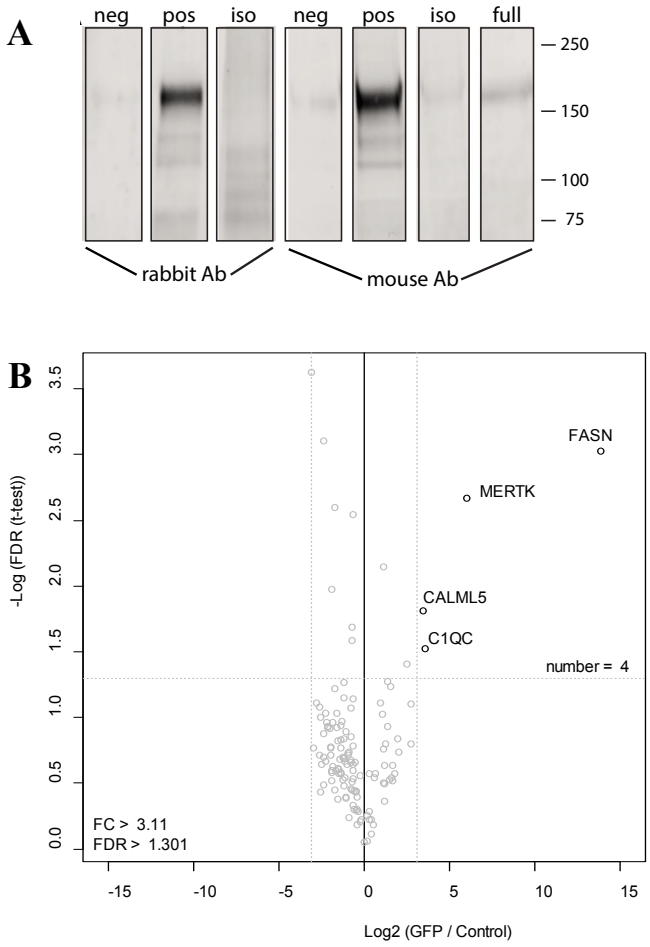

Figure II.22: Quantitative mass spectroscopy of MerTK protein complexes. (**A**) Immunoprecipitation was performed on the cytoplasmic of day 0 DCs. Using 2 different α-MerTK antibodies (rabbit and mouse) MerTK was pulled down and stained in the 'pos' lanes. The 'neg' lanes contain the cytoplasmic fraction after MerTK pulldown, and are indeed deprived of MerTK as expected. Pulldown with an aspecific mouse/rabbit antibody (iso) also correctly resulted in a negative MerTK staining with the rabbit antibody showing some background noise. Comparing the intensity of the MerTK band in the 'pos' lanes to the 'full' lane is an indication of the efficiency of the MerTK IP. Performing a similar western blot assessment of the efficiency of the MerTK in the nuclear fraction was not possible due to the lack of enough cellular material and challenging experiments. (**B**) Typical volcano-plot displaying the results of the LS-MS performed on the cytoplasmic MerTK-protein complexes. The ratio between signal obtained with the aspecific antibody (iso in A) and the signal obtained with the α-MerTK antibody determines the degree of enrichment. The proteins found in the right upper quadrant are significantly enriched. The same experiment was performed on MerTK-protein complexes IPed from the nucleus, but the volcanoplot did not yield any significantly enhanced proteins, and the total amount of proteins found in the sample was also very low.

Possible ways to further strengthen our model include performing quantitative mass spectroscopy on protein complexes that nuclear MerTK is part of. Quantitative liquid-chromatography mass spectroscopy (LC-MS) allows for the identification of enriched proteins within a solution without the need to focus on previously defined candidates[108]. Identifying well-known nuclear factors associated to MerTK will be indicative of its function. A transcription factor would for example be expected to strongly associate with proteins from the multiprotein complex RNApolII, one of the key molecules in transcribing DNA into RNA. Nuclear proteins complexes that include MerTK can be obtained by performing Immunoprecipitation (IP) in the nuclear fraction of DCs highly expressing nuclear MerTK. We performed initial experiments along these lines and successfully IPed MerTK in the cytoplasmic fraction of DCs (Fig. II.22 A). We then applied the same strategy, using the mouse antibody (better ratio between positive and aspecific 'iso' signal) to IP nuclear MerTK, and performed quantitative mass spectroscopy on MerTK from both cytoplasmic and nuclear fractions. Figure II.22 B shows the results obtained from the cytoplasm, where three proteins were specifically enriched in the IP product (FASN, CALML5 and C1QC). However, for the nuclear fraction, no enriched proteins were identified, including MerTK itself. This indicates that the IP failed and MerTK was not efficiently isolated in the first place. The enormous demand for cellular material in these experiments (primary monocytes cultured for 2 days into day 0 DCs) strongly limited our options of protocol optimization for the nuclear IP. Still, it would be important to invest both time and resources, and even better with a model system that does not rely on the isolation and culturing of primary cells, to elucidate the exact function of nuclear MerTK. Subsequent identification of the genetic loci where MerTK binds using ChiP-seq approaches would then be the ultimate goal to uncover which genes and therefore cellular processes MerTK is regulating as a nuclear factor.

Multidimensional organization of the chromatin at the single cell level

Although links between the organization of the genome at the nanoscale and its functional characteristics are becoming increasingly clear, studying all aspects at the same time in the same cell remains extremely challenging. Ideally, in the case of our MerTK studies, one would want to acquire structural data about the interaction between MerTK and chromatin, and functional data on the transcriptional activity at the same time in the same genomic area. STORM super-resolution imaging and other high-resolution techniques have provided great advances in structural studies over the past decade, but recording functional data in single, intact cells with similar sensitivity is often challenging. Currently, functional experiments typically involve biochemical ensemble techniques which do not provide information of the dynamics of the processes under study.

Moreover, biochemical techniques are normally not sensitive to local effects and their ensemble working principle washout any cell-to-cell variations.

During my doctoral studies, I have often struggled in trying to add a functional dimension to the super-resolution localization data we obtained. The low availability of biophysical tools that can quantitatively report on the activity of single molecules in intact cells have been one of the main limiting factors. It is therefore that I'm greatly looking forward to work as a post-doctoral researcher in the lab of Antoine Coulon at the Curie Institute in Paris. His team aims to decipher the multi-dimensional organization of the genome by recording spatial, temporal and transcriptional information at the same time with single-cell sensitivity. This is typically done by measuring the amount of nascent RNA produced over time at a specific gene locus, while tracking its spatial exploration of the nuclear area within the same time frame. By using this strategy to look at interactions between different genes or between genes and regulatory proteins, this line of research holds great promise to gain unprecedented insight into how the dynamic organization of the genome relates to transcriptional activity.

II.6 Conclusions

In this thesis, we aimed to unravel the spatial distribution of tyrosine kinase receptor MerTK in human dendritic cells (DCs) to further the understanding of its molecular functioning. Specifically, we: 1) Mapped the spatial organization of MerTK on the membrane of tolerogenic DCs, 2) Characterized the intracellular pool of MerTK, 3) Identified the role of ligand binding and thus receptor activation in the subcellular distribution of MerTK and 4) Determined the interaction and spatial relation between intracellular MerTK and other proteins of interest in order to uncover its intracellular function.

We have for the first time, to our knowledge, characterized the spatial distribution of MerTK on the plasma membrane of tolerogenic DCs at the nanometre scale using STED nanoscopy. We found that the receptor organizes in small, well-separated nanoclusters that are homogeneously distributed on the plasma membrane of human DCs. The clusters contained on average 3 MerTK molecules each, but larger clusters consisting of up to 11 receptors per cluster were occasionally found as well. Moreover, we demonstrated that the intracellular pool of MerTK is mainly located in the nucleus, regardless of whether the DCs have a tolerogenic or immunogenic phenotype. We discovered that the degree of nuclear localization strictly depends on DC maturation, uniquely indicating a physiological function for the nuclear translocation of a RTK in the context of immunity.

In addition, we showed that intracellular MerTK strongly colocalizes with ligand ProS, and that ProS accumulates to the nucleus with a same dependence on DC differentiation as demonstrated for MerTK. Nuclear translocation of MerTK was furthermore reduced when ligand availability in the medium is limited. Ligand-activated intracellular MerTK was found to significantly accumulate into the ER, indicating that the ligand-dependent nuclear translocation of MerTK routes through this subcellular compartment.

The endocytic receptor LRP-1 was furthermore identified as a chaperone in this process. LRP-1 was also found to localize to the nucleus of DCs, and strong intracellular colocalization between MerTK and LRP-1 was observed. MerTK associated to the nuclear envelope at the final stages of translocation was almost exclusively found to be associated to LRP-1. We established a direct correlation between the amount of nuclear MerTK and nuclear LRP-1 in the nucleus, and nuclear translocation of MerTK was significantly reduced when LRP-1 expression by DCs was low. Therefore, our data implicates LRP-1 for the first time in regulating the translocation of any tyrosine kinase receptor, and might thus have a great impact on the understanding of and possible interference with the oncogenic translocation of other RTKs.

We finally characterized the nanoscale spatial relationship between MerTK and chromatin within the nucleus of intact DCs using STORM super-resolution microscopy. Our data suggest that nuclear MerTK interacts with transcriptionally active genomic regions, and that nuclear accumulation of MerTK is more pronounced when the chromatin of DCs in displaying a more open and accessible conformation consistent with globally increased transcriptional activity. This possibly points towards a role for MerTK as a transcription factor regulating the differentiation of dendritic cells during early stages. All together our work thus provides compelling evidence that RTKs can display a physiologically relevant function in healthy, non-proliferative cells, and provides the critical first steps towards a more thorough understanding of the molecular mechanism of action of nuclear MerTK.

.

II.7 References

1. Linger RMA, Keating AK, Earp HS, Graham DK. TAM receptor tyrosine kinases: biologic functions, signaling, and potential therapeutic targeting in human cancer. *Adv. Cancer Res.* 2008;100:35–83.
2. Cummings CT, DeRyckere D, Earp HS, Graham DK. Molecular Pathways: MERTK Signaling in Cancer. *Clin. Cancer Res.* 2013;19(19):5275–5280.
3. Graham DK, DeRyckere D, Davies KD, Earp HS. The TAM family: phosphatidylserine-sensing receptor tyrosine kinases gone awry in cancer. *Nat. Rev. Cancer*. 2014;14(12):769–785.
4. Camenisch TD, Koller BH, Earp HS, Matsushima GK. A novel receptor tyrosine kinase, Mer, inhibits TNF-alpha production and lipopolysaccharide-induced endotoxic shock. *J. Immunol.* 1999;162(6):3498–503.
5. Scott RS, McMahon EJ, Pop SM, et al. Phagocytosis and clearance of apoptotic cells is mediated by MER. *Nature*. 2001;411(6834):207–211.
6. Lu Q, Lemke G. Homeostatic Regulation of the Immune System by Receptor Tyrosine Kinases of the Tyro 3 Family. *Science (80-.).* 2001;293(5528):306–311.
7. Rothlin C V, Ghosh S, Zuniga EI, Oldstone MB a, Lemke G. TAM receptors are pleiotropic inhibitors of the innate immune response. *Cell*. 2007;131(6):1124–36.
8. Wallet MA, Sen P, Flores RR, et al. MerTK is required for apoptotic cell–induced T cell tolerance. *J. Exp. Med.* 2008;205(1):219–232.
9. Rothlin C V, Lemke G. TAM receptor signaling and autoimmune disease. *Curr. Opin. Immunol.* 2010;22(6):740–6.
10. Cabezón R, Carrera-Silva EA, Flórez-Grau G, et al. MERTK as negative regulator of human T cell activation. *J. Leukoc. Biol.* 2015;97(4):751–60.
11. Behrens EM, Gadue P, Gong S, et al. The mer receptor tyrosine kinase: expression and function suggest a role in innate immunity. *Eur. J. Immunol.* 2003;33(8):2160–2167.
12. Sen P, Wallet MA, Yi Z, et al. Apoptotic cells induce Mer tyrosine kinase-dependent blockade of NF-kappaB activation in dendritic cells. *Blood*. 2007;109(2):653–60.
13. Keating A, Linger R, Graham D. MERTK (c-mer proto-oncogene tyrosine kinase). *Atlas Genet. Cytogenet. Oncol. Haematol.* 2011;13(10):728–732.
14. Sather S, Kenyon KD, Lefkowitz JB, et al. A soluble form of the Mer receptor tyrosine kinase inhibits macrophage clearance of apoptotic cells and platelet aggregation. *Blood*. 2007;109(3):1026–1033.
15. Ling L, Templeton D, Kung HJ. Identification of the major autophosphorylation sites of Nyk/Mer, an NCAM-related receptor tyrosine kinase. *J. Biol. Chem.* 1996;271(31):18355–62.
16. Prasad D, Rothlin CV, Burrola P, et al. TAM receptor function in the retinal pigment epithelium. *Mol. Cell. Neurosci.* 2006;33(1):96–108.
17. Carrera Silva E a, Chan PY, Joannas L, et al. T cell-derived protein S engages TAM receptor signaling in dendritic cells to control the magnitude of the immune response. *Immunity*. 2013;39(1):160–70.
18. Zagórska A, Través PG, Lew ED, Dransfield I, Lemke G. Diversification of TAM receptor tyrosine kinase function. *Nat. Immunol.* 2014;15:920–928.
19. Nagata K, Ohashi K, Nakano T, et al. Identification of the product of growth arrest-specific gene 6 as a common ligand for Axl, Sky, and Mer receptor tyrosine kinases. *J. Biol. Chem.* 1996;271(47):30022–7.
20. Chen J, Carey K, Godowski PJ. Identification of Gas6 as a ligand for Mer, a neural cell adhesion molecule related receptor tyrosine kinase implicated in cellular transformation. *Oncogene*. 1997;14(17):2033–2039.
21. Caberoy NB, Zhou Y, Li W. Tubby and tubby-like protein 1 are new MerTK ligands for

phagocytosis. *EMBO J.* 2010;29(23):3898–910.
22. Caberoy, Nora B, Alvarado, Gabriela, Bigcas Jo-Lawrence, Li W. Galectin-3 is a new MerTK-specific eat-me signal. *J Cell Physiol*. 2012;227(2):401–407.
23. Burstyn-Cohen T, Heeb MJ, Lemke G. Lack of protein S in mice causes embryonic lethal coagulopathy and vascular dysgenesis. *J. Clin. Invest.* 2009;119(10):2942–53.
24. Ekman C, Stenhoff J, Dahlbäck B. Gas6 is complexed to the soluble tyrosine kinase receptor Axl in human blood. *J. Thromb. Haemost.* 2010;8(4):838–844.
25. Anderson HA, Maylock CA, Williams JA, et al. Serum-derived protein S binds to phosphatidylserine and stimulates the phagocytosis of apoptotic cells. *Nat. Immunol.* 2003;4(1):87–91.
26. Phillips BE, Garciafigueroa Y, Trucco M, Giannoukakis N. Clinical Tolerogenic Dendritic Cells: Exploring Therapeutic Impact on Human Autoimmune Disease. *Front. Immunol.* 2017;8:1279.
27. Giannoukakis N. Tolerogenic dendritic cells for Type 1 diabetes. *Immunotherapy*. 2013;5(6):569–571.
28. Bell GM, Anderson AE, Diboll J, et al. Autologous tolerogenic dendritic cells for rheumatoid and inflammatory arthritis. *Ann. Rheum. Dis.* 2017;76(1):227–234.
29. Benham H, Nel HJ, Law SC, et al. Citrullinated peptide dendritic cell immunotherapy in HLA risk genotype–positive rheumatoid arthritis patients. *Sci. Transl. Med.* 2015;7(290):290ra87-290ra87.
30. Jauregui-Amezaga A, Cabezón R, Ramírez-Morros A, et al. Intraperitoneal Administration of Autologous Tolerogenic Dendritic Cells for Refractory Crohn's Disease: A Phase I Study. *J. Crohn's Colitis*. 2015;9(12):1071–1078.
31. Holland SJ, Powell MJ, Franci C, et al. Multiple roles for the receptor tyrosine kinase axl in tumor formation. *Cancer Res.* 2005;65(20):9294–303.
32. Mahadevan D, Cooke L, Riley C, et al. A novel tyrosine kinase switch is a mechanism of imatinib resistance in gastrointestinal stromal tumors. *Oncogene*. 2007;26(27):3909–3919.
33. Vajkoczy P, Knyazev P, Kunkel A, et al. Dominant-negative inhibition of the Axl receptor tyrosine kinase suppresses brain tumor cell growth and invasion and prolongs survival. *Proc. Natl. Acad. Sci. U. S. A.* 2006;103(15):5799–804.
34. Wells A, Marti U. Signalling shortcuts: cell-surface receptors in the nucleus? *Nat. Rev. Mol. Cell Biol.* 2002;3:1–6.
35. Chen M-K, Hung M-C. Proteolytic cleavage, trafficking, and functions of nuclear receptor tyrosine kinases. *FEBS J.* 2015;282(19):3693–721.
36. Carpenter G, Liao H-J. Trafficking of receptor tyrosine kinases to the nucleus. *Exp. Cell Res.* 2009;315(9):1556–66.
37. Wang Y-N, Wang H, Yamaguchi H, et al. COPI-mediated retrograde trafficking from the Golgi to the ER regulates EGFR nuclear transport. *Biochem. Biophys. Res. Commun.* 2010;399(4):498–504.
38. Wang Y-N, Hung M-C. Nuclear functions and subcellular trafficking mechanisms of the epidermal growth factor receptor family. *Cell Biosci.* 2012;2(1):13.
39. Lin S-Y, Makino K, Xia W, et al. Nuclear localization of EGF receptor and its potential new role as a transcription factor. *Nat. Cell Biol.* 2001;3(9):802–808.
40. Johnson HM, Subramaniam PS, Olsnes S, Jans DA. Trafficking and signaling pathways of nuclear localizing protein ligands and their receptors. *BioEssays*. 2004;26(9):993–1004.
41. Reilly JF, Maher PA. Importin beta-mediated nuclear import of fibroblast growth factor receptor: role in cell proliferation. *J. Cell Biol.* 2001;152(6):1307–12.
42. Wang YN, Yamaguchi H, Huo L, et al. The translocon Sec61β localized in the inner nuclear membrane transports membrane-embedded EGF receptor to the nucleus. *J. Biol. Chem.* 2010;285:38720–38729.

43. Chaumet A, Wright GD, Seet SH, et al. ARTICLE Nuclear envelope-associated endosomes deliver surface proteins to the nucleus. *Nat. Commun.* 2015;6:8218.
44. Hong-Jun Liao GC. Role of the Sec61 Translocon in EGF Receptor Trafficking to the Nucleus and Gene Expression. *Mol. Biol. Cell*. 2007;18(March):1064–1072.
45. Wang Y-N, Yamaguchi H, Hsu J-M, Hung M-C. Nuclear trafficking of the epidermal growth factor receptor family membrane proteins. *Oncogene*. 2010;29(28):3997–4006.
46. Migdall-Wilson J, Bates C, Schlegel J, et al. Prolonged exposure to a Mer ligand in leukemia: Gas6 favors expression of a partial Mer glycoform and reveals a novel role for Mer in the nucleus. *PLoS One*. 2012;7(2):e31635.
47. Liu HS, Hsu PY, Lai MD, et al. An unusual function of RON receptor tyrosine kinase as a transcriptional regulator in cooperation with EGFR in human cancer cells. *Carcinogenesis*. 2010;31(8):1456–1464.
48. Huo L, Wang Y-N, Xia W, et al. RNA helicase A is a DNA-binding partner for EGFR-mediated transcriptional activation in the nucleus. *Proc. Natl. Acad. Sci. U. S. A.* 2010;107(37):16125–30.
49. Wang S-C, Nakajima Y, Yu Y-L, et al. Tyrosine phosphorylation controls PCNA function through protein stability. *Nat. Cell Biol.* 2006;8(12):1359–1368.
50. Liccardi G, Hartley JA, Hochhauser D. EGFR Nuclear Translocation Modulates DNA Repair following Cisplatin and Ionizing Radiation Treatment. *Cancer Res.* 2011;71(3):1103–1114.
51. Verma A, Warner SL, Vankayalapati H, Bearss DJ, Sharma S. Targeting Axl and Mer Kinases in Cancer. *Mol. Cancer Ther.* 2011;10(10):1763–1773.
52. van Zanten TS, Cambi A, Koopman M, et al. Hotspots of GPI-anchored proteins and integrin nanoclusters function as nucleation sites for cell adhesion. *Proc. Natl. Acad. Sci. U. S. A.* 2009;106(44):18557–62.
53. Garcia-Parajo MF, Cambi A, Torreno-Pina JA, Thompson N, Jacobson K. Nanoclustering as a dominant feature of plasma membrane organization. *J. Cell Sci.* 2014;127(23):4995–5005.
54. Torreno-Pina JA, Manzo C, Salio M, et al. The actin cytoskeleton modulates the activation of iNKT cells by segregating CD1d nanoclusters on antigen-presenting cells. *Proc. Natl. Acad. Sci. U. S. A.* 2016;113(6):E772-81.
55. Torreno-Pina JA, Castro BM, Manzo C, et al. Enhanced receptor-clathrin interactions induced by N-glycan-mediated membrane micropatterning. *Proc. Natl. Acad. Sci. U. S. A.* 2014;111(30):11037–42.
56. de Vries IJM, Adema GJ, Punt CJA, Figdor CG, Figdor CG. Phenotypical and Functional Characterization of Clinical-Grade Dendritic Cells. *Adopt. Immunother.* 2005;113–126.
57. Wang Y, Huo L, Hsu JL, Hung M. Nuclear G-Protein Coupled Receptors. *Methods Mol. Biol.* 2015;1234:99–112.
58. Rust MJ, Bates M, Zhuang X. Sub-diffraction-limit imaging by stochastic optical reconstruction microscopy (STORM). *Nat. Methods*. 2006;3(10):793–796.
59. Bates M, Huang B, Dempsey GT, Zhuang X. Multicolor Super-Resolution Imaging with Photo-Switchable Fluorescent Probes. *Science (80-.).* 2007;317(5845):1749–1753.
60. Ricci MA, Manzo C, Garcia-Parajo MF, Lakadamyali M, Cosma MP. Chromatin fibers are formed by heterogeneous groups of nucleosomes in vivo. *Cell*. 2015;160(6):1145–1158.
61. Dani A, Huang B, Bergan J, Dulac C, Zhuang X. Superresolution imaging of chemical synapses in the brain. *Neuron*. 2010;68(5):843–56.
62. Rizk A, Paul G, Incardona P, et al. Segmentation and quantification of subcellular structures in fluorescence microscopy images using Squassh. *Nat. Protoc.* 2014;9(3):586–596.
63. Brand TM, Iida M, Li C, Wheeler DL. Network and its Role in Cancer. *Discov. Med.* 2012;12(66):419–432.

64. Berges C, Naujokat C, Tinapp S, et al. A cell line model for the differentiation of human dendritic cells. *Biochem. Biophys. Res. Commun.* 2005;333(3):896–907.
65. Guo Q, Zhang L, Li F, Jiang G. The plasticity and potential of leukemia cell lines to differentiate into dendritic cells. *Oncol. Lett.* 2012;4(4):595–600.
66. Stitt TN, Conn G, Gore M, et al. The anticoagulation factor protein S and its relative, Gas6, are ligands for the Tyro 3/Axl family of receptor tyrosine kinases. *Cell*. 1995;80(4):661–70.
67. Lemke G, Rothlin C V. Immunobiology of the TAM receptors. *Nat. Rev. Immunol.* 2008;8(5):327–36.
68. Subramanian M, Hayes CD, Thome JJ, et al. An AXL/LRP-1/RANBP9 complex mediates DC efferocytosis and antigen cross-presentation in vivo. *J. Clin. Invest.* 2014;124(3):1296–1308.
69. Dekker J, Misteli T. Long-range chromatin interactions. *Cold Spring Harb. Perspect. Biol.* 2015;7(10):.
70. Kosak ST, Skok JA, Medina KL, et al. Subnuclear Compartmentalization of Immunoglobulin Loci During Lymphocyte Development. *Science (80-.).* 2002;296(5565):158–162.
71. Finlan LE, Sproul D, Thomson I, et al. Recruitment to the Nuclear Periphery Can Alter Expression of Genes in Human Cells. *PLoS Genet.* 2008;4(3):e1000039.
72. Reddy KL, Zullo JM, Bertolino E, Singh H. Transcriptional repression mediated by repositioning of genes to the nuclear lamina. *Nature*. 2008;452(7184):243–247.
73. Guelen L, Pagie L, Brasset E, et al. Domain organization of human chromosomes revealed by mapping of nuclear lamina interactions. *Nature*. 2008;453(7197):948–951.
74. Kind J, van Steensel B. Genome–nuclear lamina interactions and gene regulation. *Curr. Opin. Cell Biol.* 2010;22(3):320–325.
75. Karnavas T, Pintonello L, Agresti A, Bianchi ME. Histone content increases in differentiating embryonic stem cells. *Front. Physiol.* 2014;5:330.
76. Pereira CF, Rossy J, Owen DM, Mak J, Gaus K. HIV taken by STORM: Super-resolution fluorescence microscopy of a viral infection. *Virol. J.* 2012;9(1):84.
77. Rossy J, Owen DM, Williamson DJ, Yang Z, Gaus K. Conformational states of the kinase Lck regulate clustering in early T cell signaling. *Nat. Immunol.* 2013;14(1):82–89.
78. Sherman E, Barr V, Manley S, et al. Functional Nanoscale Organization of Signaling Molecules Downstream of the T Cell Antigen Receptor. *Immunity*. 2011;35:705–720.
79. Roh K-H, Lillemeier BF, Wang F, Davis MM. The coreceptor CD4 is expressed in distinct nanoclusters and does not colocalize with T-cell receptor and active protein tyrosine kinase p56lck. *Proc. Natl. Acad. Sci. U. S. A.* 2015;112(13):E1604-13.
80. Cebecauer M, Spitaler M, Serge A, Magee AI. Signalling complexes and clusters: functional advantages and methodological hurdles. *J. Cell Sci.* 2010;123(3):309–320.
81. Lagerholm BC, Thompson NL. Theory for Ligand Rebinding at Cell Membrane Surfaces. *Biophys. J.* 1998;74(3):1215–1228.
82. Diez-Ahedo R, Normanno D, Esteban O, et al. Dynamic Re-organization of Individual Adhesion Nanoclusters in Living Cells by Ligand-Patterned Surfaces. *Small*. 2009;5(11):1258–1263.
83. Grakoui A, Bromley SK, Sumen C, et al. The immunological synapse: a molecular machine controlling T cell activation. *Science (80-.).* 1999;285(5425):221–227.
84. Cabezón R, Ricart E, España C, Panés J, Benitez-Ribas D. Gram-negative enterobacteria induce tolerogenic maturation in dexamethasone conditioned dendritic cells. *PLoS One*. 2012;7(12):e52456.
85. Heldin C-H, Ericsson J. RIPping Tyrosine Kinase Receptors Apart. *Science (80-.).* 2001;294(5549):2111–2113.
86. Ni C-Y. gamma -Secretase Cleavage and Nuclear Localization of ErbB-4 Receptor Tyrosine Kinase. *Science (80-.).* 2001;294(5549):2179–2181.

87. Katoh M, Hattori Y, Sasaki H, et al. K-sam gene encodes secreted as well as transmembrane receptor tyrosine kinase. *Proc. Natl. Acad. Sci. U. S. A.* 1992;89(7):2960–4.
88. Wells A, Marti U. Signalling shortcuts: cell-surface receptors in the nucleus? *Nat. Rev. Mol. Cell Biol.* 2002;3(September):1–6.
89. Karsten V, Hegde RS, Sinai AP, Yang M, Joiner KA. Transmembrane domain modulates sorting of membrane proteins in Toxoplasma gondii. *J. Biol. Chem.* 2004;279(25):26052–7.
90. Longo N, Shuster RC, Griffin LD, Langley SD, Elsas LJ. Activation of insulin receptor signaling by a single amino acid substitution in the transmembrane domain. *J. Biol. Chem.* 1992;267(18):12416–9.
91. Myers JM, Martins GG, Ostrowski J, Stachowiak MK. Nuclear trafficking of FGFR1: A role for the transmembrane domain. *J. Cell. Biochem.* 2003;88(6):1273–1291.
92. Albi E, Magni MPV. The role of intranuclear lipids. *Biol. Cell*. 2004;96(8):657–667.
93. Cascianelli G, Villani M, Tosti M, et al. Lipid microdomains in cell nucleus. *Mol. Biol. Cell*. 2008;19(12):5289–95.
94. Irvine R. Nuclear Lipid Signaling. *Sci. Signal.* 2000;(48):.
95. Schmahl J. Fgf9 induces proliferation and nuclear localization of FGFR2 in Sertoli precursors during male sex determination. *Development*. 2004;131(15):3627–3636.
96. Herz J, Strickland DK. LRP: A multifunctional scavenger and signaling receptor. *J. Clin. Invest.* 2001;108(6):779–784.
97. Gonias SL, Wu L, Salicioni AM. Low density lipoprotein receptor-related protein: regulation of the plasma membrane proteome. *Thromb. Haemost.* 2004;91(6):1056–1064.
98. Theret L, Jeanne A, Langlois B, et al. Identification of LRP-1 as an endocytosis and recycling receptor for β1-integrin in thyroid cancer cells. *Oncotarget*. 2017;8(45):.
99. Wujak L, Böttcher RT, Pak O, et al. Low density lipoprotein receptor‐related protein 1 couples β1 integrin activation to degradation. *Cell. Mol. Life Sci.* 2018;75:1671–1685.
100. Perrot G, Langlois B, Devy J, et al. LRP-1-CD44, a New Cell Surface Complex Regulating Tumor Cell Adhesion. *Mol. Cell. Biol.* 2012;32(16):3293–3307.
101. Zessin PJM, Finan K, Heilemann M. Super-resolution fluorescence imaging of chromosomal DNA. *J. Struct. Biol.* 2012;177(2):344–348.
102. Boettiger AN, Bintu B, Moffitt JR, et al. Super-resolution imaging reveals distinct chromatin folding for different epigenetic states. *Nature*. 2016;529(7586):418–22.
103. Lakadamyali M, Cosma MP. Advanced microscopy methods for visualizing chromatin structure. *FEBS Lett.* 2015;589(20):3023–3030.
104. Raj N, Attardi LD. The Transactivation Domains of the p53 Protein. *Cold Spring Harb. Perspect. Med.* 2017;7(1):a026047.
105. Wärnmark A, Treuter E, Wright APH, Gustafsson J-Å. Activation Functions 1 and 2 of Nuclear Receptors: Molecular Strategies for Transcriptional Activation. *Mol. Endocrinol.* 2003;17(10):1901–1909.
106. Piskacek S, Gregor M, Nemethova M, et al. Nine-amino-acid transactivation domain: Establishment and prediction utilities. *Genomics*. 2007;89(6):756–768.
107. Piskacek M, Havelka M, Rezacova M, Knight A. The 9aaTAD transactivation domains: From Gal4 to p53. *PLoS One*. 2016;11(9):.
108. Vermeulen M, Hubner NC, Mann M. High confidence determination of specific protein–protein interactions using quantitative mass spectrometry. *Curr. Opin. Biotechnol.* 2008;19(4):331–337.